

© Copyright by Ravi teja Nallapu 2012
All Rights Reserved

Orbit Propagation via MRQ Sphere Technique

A Thesis

Presented to

the Faculty of the Department of Mechanical Engineering
University of Houston

In Partial Fulfillment

of the Requirements for the Degree

Master of Science

in Aerospace Engineering

by

Ravi teja Nallapu

August 2012

Orbit Propagation via MRQ-Sphere Technique

Ravi teja Nallapu

Approved:

Committee Members:

Chair of the committee,
Dr. Karolos Grigoriadis,
Professor,
Mechanical Engineering

Co-Chair of the committee,
Dr. Robert Provence,
Adjunct Professor,
Electrical and Computers Engineering

Dr. Jagannatha Rao,
Associate Professor,
Mechanical Engineering

Dr. Suresh Khator,
Associate Dean,
Cullen College of Engineering

Dr. Karolos Grigoriadis,
Professor and Director of Interdisciplinary
Program in Aerospace Engineering

Acknowledgements

I owe my deepest gratitude to Dr. Robert Provence for giving me the opportunity to pursue my thesis in my favorite field of Astrophysics under his esteemed guidance. His help gave me the understanding of the basics of Astrodynamics and also made me channel my research.

I owe my deepest thanks to Dr. Karolos Grigoriadis for supervising my research. His timely inputs improved the quality of my research and helped me keep track of my progress. I also owe a debt of gratitude to Dr. Grigoriadis for presenting me with numerous research opportunities including the Lunabotics Mining Competition at the NASA Kennedy Space Center.

I would also like to thank Dr. Jagannatha Rao for accepting my invitation to be a part of my thesis committee and also for being my teacher. His teaching made calculus more friendly than ever.

Special thanks goes to Dr. Brandon Jones from the University of Colorado for his support in helping me verify my computations, supplying the required information, along with guiding me throughout the project.

I would also like to take this opportunity to thank my mother, Veena Nallapu and father, Prahlad Nallapu, for providing me with an opportunity to explore my passions. Thank you very much for your love and support.

It gives me great pleasure to thank all of my friends, colleagues, teammates, students and those who in some way provided insight, suggestions, information, support and fun: Priyanka, Deepak, Sridhar, Ravi Krishna, Ganapathy, Nitin, Sneha, Shiva, Preetham, Radha Krishna, Roshan, etc. Also a special thanks goes to Eric Stern and Kiet Luong from the Engineering Computing Center for rescuing my thesis files when I almost lost all hope.

Orbit Propagation via MRQ Sphere Technique

An Abstract

of a

Thesis

Presented to

the Faculty of the Department of Mechanical Engineering

University of Houston

In Partial Fulfillment

of the Requirements for the Degree

Master of Science

in Aerospace Engineering

by

Ravi teja Nallapu

August 2012

Abstract

The Multi-Resolution Quadrature (MRQ) Sphere model, is a newly developed multi- resolution gravity model designed to estimate the gravity fields of arbitrary shaped space bodies, such as asteroids. The MRQ Sphere model uses two recently developed mathematical techniques to approximate the standard spherical harmonics. One of these tools approximates the radial decay terms using the sum of Gaussians, while the other is used for estimating the angular functions on the nodes of the quadratures of a sphere. In this work, we apply the MRQ sphere technique to the classic orbit propagation problem and compare the propagated orbit with that generated by the spherical harmonics method. We validate the methods with Earth as the primary body, and propagate the orbit of test cases such as the LAser GEOdynamics Satellite-II (LAGEOS-II) and the GPS BIIA-10 (PRN 32) satellite. We find that the MRQ-Sphere model may be applicable to orbit propagation up to a user dependent approximation.

Table of Contents

Acknowledgements	v
Abstract	vii
Table of Contents	viii
List of Figures	x
List of Tables	xiii
Chapter 1 Introduction	1
1.1 Gravity Potential	1
1.2 Perturbations	2
1.2.1 Sources	3
1.3 Coordinate Frames	5
1.3.1 Earth Centered Inertial	6
1.3.2 Earth Centered Earth Fixed	6
1.4 State Vector	7
1.4.1 Cartesian Components	8
1.4.2 Keplerian Elements	8
1.5 Orbit Propagation	11
1.5.1 Cowell's Method	11
1.6 LAGEOS-II	12
1.7 GPS BIIA-10	13
Chapter 2 Spherical Harmonics Model	14
2.1 Description	14
2.2 Model Configuration	14
2.2.1 Gravity Coefficients	15
2.2.2 Derived Legendre Functions	15
2.2.3 Formulation	16
Chapter 3 MRQ-Sphere model	18

3.1	Introduction	18
3.2	Formulation	19
3.2.1	Quadratures on the Sphere	19
3.2.2	Approximation by Gaussians	25
3.3	Model	26
3.3.1	Potential Function	26
3.3.2	Acceleration Vector	26
3.4	Model Configuration	27
Chapter 4	Results	33
4.1	Gravity Estimation	33
4.2	Orbit Propagation Results	35
4.2.1	Keplerian Elements	36
4.2.2	Cartesian Variation	41
4.2.3	Impact of the Number of Shells	43
4.2.4	Impact of the Radial Decay Accuracy	45
4.3	GPS BIIA-10 Results	47
4.3.1	Gravity Vector	47
4.3.2	Orbit Propagation	48
4.3.3	Impact of the Number of Nodes	49
4.4	Computation Time	51
4.5	Conclusion	52
4.6	Future Work	52
References	53

List of Figures

Figure 1.1	Most accurate model of the Geoid modeled according to the data collected by the GOCE satellite.	4
Figure 1.2	J2000 reference frame,courtesy: <i>civilliancomms</i>	6
Figure 1.3	Earth Centered Earth Fixed frame,courtesy: <i>Wikipedia</i>	7
Figure 1.4	Orbital elements, courtesy <i>Spaceflight.nasa.gov</i>	10
Figure 3.1	Nodes used for the orbit propagation. ($2N = 40, M = 612$)	22
Figure 3.2	Plots of the Kernel matrix and its partial derivative as a function of angle between the two unit vectors	24
Figure 3.3	Error between the radial decay and the gaussian approximation for $j_{min} = -13, j_{max} = 12, h = 0.3435$, and $\rho = \rho_{min} = 1.8799$. . .	29
Figure 3.4	Error between the radial decay and the gaussian approximation for $j_{min} = -20, j_{max} = 17, h = 0.2487$, and $\rho = \rho_{min} = 1.8799$. . .	30
Figure 3.5	Error between the radial decay and the gaussian approximation for $j_{min} = -13, j_{max} = 7, h = 0.3465$, and $\rho = \rho_{min} = 4.1141$	31
Figure 4.1	Gravity as predicted by spherical harmonics and the MRQ Sphere model.	34
Figure 4.2	Error response of the MRQ sphere acceleration gravity as compared to the Spherical Harmonics gravity.	35
Figure 4.3	Plot showing the variation of semi major axis as predicted by the MRQ Sphere model and Spherical harmonics and the error between the two models.	36
Figure 4.4	Plot showing the variation of eccentricity as predicted by the MRQ Sphere model and Spherical harmonics and the error between the two models.	37

Figure 4.5	Plot showing the variation of inclination as predicted by the MRQ Sphere model and Spherical harmonics and the error between the two models.	38
Figure 4.6	Plot showing the variation of longitude of the ascending node as predicted by the MRQ Sphere model and Spherical harmonics and the error between the two models.	39
Figure 4.7	Plot showing the variation of argument of perigee as predicted by the MRQ Sphere model and Spherical harmonics and the error between the two models.	40
Figure 4.8	Plot showing the variation of true anomaly at epoch as predicted by the MRQ Sphere model and Spherical harmonics and the error between the two models.	41
Figure 4.9	Plot showing the variation position response as predicted by the MRQ Sphere model and Spherical harmonics and the error between the two models.	42
Figure 4.10	Plot showing the variation position response as predicted by the MRQ Sphere model and Spherical harmonics and the error between the two models.	43
Figure 4.11	Plot showing impact of number of shells on the position of the satellite predicted by the model.	44
Figure 4.12	Plot showing impact of number of shells on the velocity predicted by the model.	44
Figure 4.13	Plot showing impact of radial accuracy on the position of the satellite predicted by the model.	45
Figure 4.14	Plot showing impact of radial accuracy on the velocity predicted by the model.	46

Figure 4.15 Plot showing error in position and velocity of LAGEOS-II between the accuracy improved MRQ sphere model and the spherical harmonics.	46
Figure 4.16 Plot showing the variation of gravity as predicted by the MRQ Sphere model and Spherical harmonics and the error between the two models.	47
Figure 4.17 Plot showing the variation of position of GPS IIA-10 , as predicted by the MRQ Sphere model and Spherical harmonics and the error between the two models.	48
Figure 4.18 Plot showing the variation of velocity of GPS BIIA-10, as predicted by the MRQ Sphere model and Spherical harmonics and the error between the two models.	49
Figure 4.19 Plot showing impact of number of nodes on the position of the satellite predicted by the model.	50
Figure 4.20 Plot showing impact of number of nodes on the velocity predicted by the model.	50

List of Tables

Table 3.1	Data points used for computing initial Gaussian stepsize, Jones [10].	27
Table 3.2	Data points used for computing initial Gaussian stepsize, Jones[10].	28
Table 3.3	Configuration for the MRQ sphere model representation of LAGEOS-II.	32
Table 3.4	Configuration for the MRQ sphere model representation of GPS BIIA-10.	32
Table 4.1	Propagation computation times recorded on an i-3 processor, with 4 gigabytes of RAM.	51

CHAPTER 1 INTRODUCTION

In this research, we study the application of a newly developed multi-resolution representation of gravity potential called the MRQ-sphere technique. This model was developed to estimate the gravity field of EROS-433 [10]. In this work we use this method to the classic orbit propagation problem for LAGEOS-II and GPS BIIA-10 satellites.

1.1 Gravity Potential

The gravitational potential at a location is defined as the work done by the gravitational force per unit mass, that is done by the gravitational force to move an object to a fixed reference location. By convention, the reference location is usually taken at infinity, so the gravitational potential is zero infinitely far away from any mass and negative at any finite distance. A potential function U is said to be a Newtonian potential if it satisfies

$$\lim_{r \rightarrow \infty} rU = GM, \quad (1.1)$$

and

$$\lim_{r \rightarrow \infty} U = 0, \quad (1.2)$$

where r is the distance at which the function is evaluated, M is the mass of the body whose potential is being evaluated, and G is Newton's universal gravitational constant [9]. The solution to the potential function is obtained by solving Laplace's equation,

$$\nabla^2 U = 0. \quad (1.3)$$

Where ∇ is the gradient operator. Then, the potential is computed by solving (1.3) on the boundary values of a space body and additional Newtonian constraints like (1.1) and (1.2) [9]. The gradient of the gravity potential gives the gravity field which is defined as the gravitational force per unit mass, which is the gravity acceleration vector, i.e.,

$$g = \nabla U. \quad (1.4)$$

However, as a special case if the body whose potential is being evaluated is a well defined sphere then the potential function becomes

$$U_{ideal} = -\frac{GM}{r}. \quad (1.5)$$

The negative sign indicates that the potential at infinity is zero. From (1.4) and (1.5) we have

$$g_{ideal} = \nabla U_{ideal}. \quad (1.6)$$

A deviation from this definition of potential is a perturbation, which will be discussed in section 1.2.

1.2 Perturbations

In this section we will briefly describe the concept of perturbation of variables. As mentioned earlier, perturbation refers to any deviation from the normal or the expected value. There are two main classes of perturbations these are called special perturbations and general perturbations. The solution to special perturbations deal with direct numerical integration techniques, while the solutions of general perturbation techniques employ analytic integration of series expansions of the perturbation terms. The perturbation term in most cases will be the acceleration. Thus we can express the true acceleration as the sum of ideal and perturbation

accelerations i.e,

$$\bar{g}_{true} = \bar{g}_{ideal} + \bar{g}_{perturbation}. \quad (1.7)$$

In the absence of perturbations, the true and ideal accelerations would be equal. The ideal acceleration is given by Newtons Universal Law of Gravitation. Let M be the mass of the central body (Earth) and m be the mass of the body orbiting the primary body (LAGEOS-II), whose centers are separated by a distance r . Then Newton's gravitational law states that

$$\bar{g}_{ideal} = -\frac{\mu}{r^3}\bar{r}, \quad (1.8)$$

where μ is the gravitational parameter given by

$$\mu = G(M + m), \quad (1.9)$$

G being the Gravitational constant. It is generally a valid assumption that mass of the central object is very large compared to that of the secondary body ($M \gg m$). Therefore it is also valid to write (1.9) as

$$\mu = GM. \quad (1.10)$$

In our computation we use

$$\mu = 398600.4415 km^3/s^2. \quad (1.11)$$

Hence, we can now write (1.7) as

$$\bar{g}_{true} = -\frac{\mu}{r^3}\bar{r} + \bar{g}_p. \quad (1.12)$$

1.2.1 Sources

Perturbation can be accounted to a number of sources. Some of these sources are discussed as follows.

Geometries of the participating bodies

The ideal acceleration in eq.(1.8) is under the assumption that r is well defined, i.e, the two participating bodies have a regular geometry and hence their center of mass can easily be defined. Since this research deals with Earth as the central body, its irregular shape is the cause of this kind of perturbation. The Earth is slightly bulged at the equator, flattened at the poles, and is asymmetric. Fig. 1.1 shows the irregular nature of the Earth's shape as modeled according to the data collected by the GOCE satellite. Hence in this case, the potential function is determined and then we compute the acceleration.

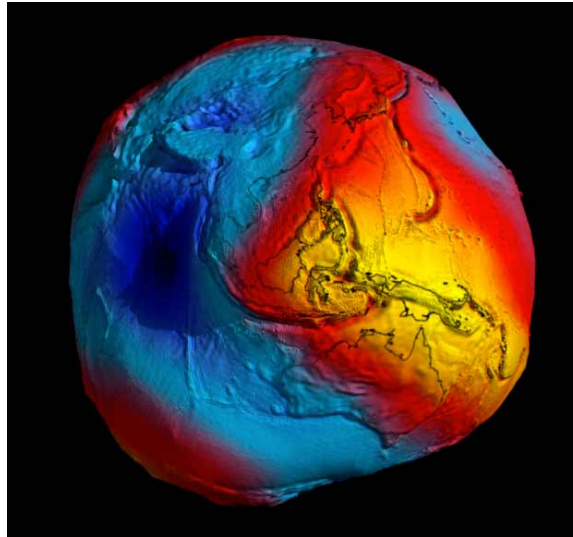


Figure 1.1. Most accurate model of the Geoid modeled according to the data collected by the GOCE satellite.

In this research we will be focusing on these kind of perturbations alone. The other types mentioned here are just to give an idea of various sources. Spherical harmonics technique is the standard technique employed to compute the potential function U . We discuss this how this is done in chapter 2 and then compute the acceleration as

$$\bar{g} = \frac{\partial U}{\partial x}. \quad (1.13)$$

However, the scope of this thesis is to replace the spherical harmonics technique with the MRQ-Sphere technique which will be discussed in chapter 3.

Atmospheric Drag

The formulation of drag depends on parameters like atmospheric fluctuations and frontal areas of the orbiting objects. Drag will always be opposite to the velocity of the vehicle relative to the atmosphere.[2]

Radiation Pressure

Though the perturbations caused by the radiation pressure are small it has a considerable effect on the large area to mass ratio satellites (like ECHO)[2].

Thrust

Thrust can be treated directly by resolving the thrust components in the x,y,z directions, and hence can be handled quite simply[2].

1.3 Coordinate Frames

In order to have a reference for the position, velocity, and acceleration vectors, we need to define a reference frame for them. There are a wide number of reference Cartesian frames depending upon the origin. We have the Geocentric frames that have the origin at the center of the Earth. Then we have topocentric-horizon frames that have their origin on the surface of the Earth. Then there are heliocentric frames that have their origin at the center of the sun. Since this research sticks to orbits around the Earth we will employ the Geocentric Cartesian frames. Geo-centric frames are further classified into two kinds.[16] They are Earth Centered Inertial (ECI) and Earth Centered Earth Fixed (ECEF), which are discussed as follows.

1.3.1 Earth Centered Inertial

Earth Centered Inertial frames are those that are at rest with respect to Earth, i.e, they do not rotate. Though the name suggests inertial these frames are not truly inertial as the Earth itself moves with respect to sun. Despite this, these frames are a suitable choice to express the position and velocity. There are a wide variety in this class of reference frames depending on the Julian date they were put into practice. In this research, we employ the J2000 reference frame or the J2k frame where the X-axis points to the J2000 vernal equinox direction, Z-Axis is perpendicular to the ecliptic, and the Y-axis completes the right-hand Cartesian frame. The ecliptic of this system is the equatorial plane of the Earth. Fig. 1.2 shows the location of axis in the J2000 frame.

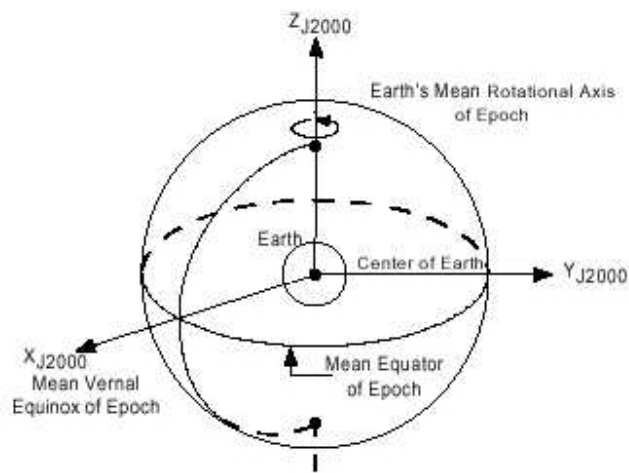


Figure 1.2. J2000 reference frame, courtesy: *civilliancomms*

1.3.2 Earth Centered Earth Fixed

Earth-Centered, Earth-Fixed, is also known as a conventional terrestrial system. Its axes are aligned with the International Reference Pole (IRP) and International Reference Meridian (IRM) that are fixed with respect to the surface of the Earth;

therefore, it is referred to as Earth-Fixed. The Z-axis points towards the north, but it does not coincide exactly with the instantaneous Earth rotational axis. The slight wobbling of the rotational axis is known as polar motion. The X-axis intersects the sphere of the Earth at the Equator (0° latitude) and the Greenwich Meridian (0° longitude). This means that ECEF rotates with the Earth and therefore, coordinates of a point fixed on the surface of the Earth do not change. Fig. 1.3 shows an ECEF frame.

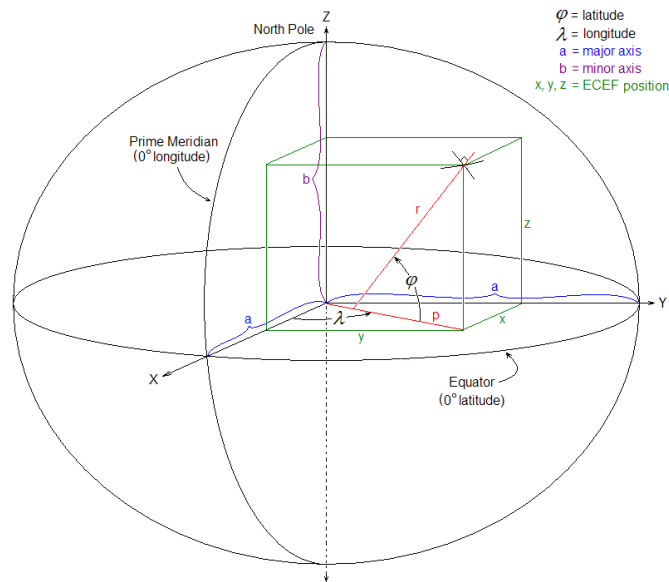


Figure 1.3. Earth Centered Earth Fixed frame,courtesy: *Wikipedia*

1.4 State Vector

A state vector holds the information (also called the state) we seek from the body of interest. In our case, the body of interest is the satellite, LAGEOS-II. The state can be the Cartesian coordinates of the position and velocity or the Keplerian orbital elements.

1.4.1 Cartesian Components

The Cartesian components are the traditional way of expressing the position and velocity. We choose a convenient coordinate frame such as ECI or the ECEF frame and define the components with respect to the origin.

1.4.2 Keplerian Elements

The Cartesian frame, though efficient, does not describe the geometry of the orbit. Hence we use six Keplerian elements to describe the position of the satellite and also the geometry of the orbit. Five of these elements completely describe the size, shape, and orientation of the orbit. The final orbital element is used to determine the instantaneous position of the satellite. These elements may be defined as follows

Semi-major axis

The semi major axis defines the linear distance from the center of the orbit to the farthest point on the orbit. It is denoted by ' a '.

Eccentricity

Mathematically it is defined as the ratio of distance between the center of the conic to its focus and the semi major axis. It is commonly denoted by ' e '.

Inclination

Inclination is defined as the angle between the Z-axis and the angular momentum vector, which is the vector perpendicular to the plane containing the radius and the velocity vectors. It is denoted by ' i '.

Longitude of the Ascending Node

The angle in the fundamental plane between the X-axis and the point where the satellite crosses the fundamental plane in a northern direction (ascending node) and is measured clockwise when viewed from the fundamental plane. It is denoted by ' Ω '.

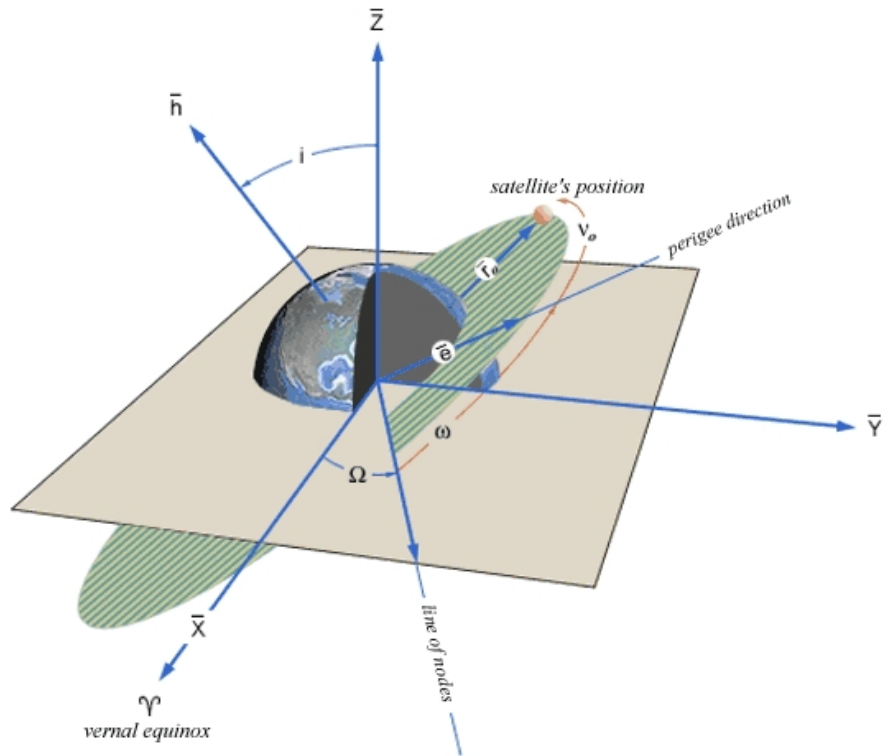
Argument of Periapsis

The angle which is in the plane of the orbit between the ascending node and the periapsis of the orbit. Periapsis is defined as the nearest vertex from the focus. It is denoted by ' ω '.

True Anomaly at Epoch

As discussed earlier, the shape and size of the orbit are defined by five of the above defined elements. The true anomaly at epoch however is used for determining the current position of the satellite. The true anomaly at epoch is defined as the angle in the plane of the orbit between periapsis and the position of the satellite at a particular time t_0 called the epoch. It is denoted by ' ν '.

Fig.1.4 shows the graphical meaning of these Keplerian elements. Depending on the data available we can choose the Cartesian coordinates or the Keplerian. We can always switch between these two modes, i.e Cartesian to Keplerian and vice-versa[2]. In this research we compute the data in Cartesian frame and then convert them to also throw a light on the Keplerian elements.



- a - defines the size of the orbit
- e - defines the shape of the orbit
- i - defines the orientation of the orbit with respect to the Earth's equator.
- ω - defines where the low point, perigee, of the orbit is with respect to the Earth's surface.
- Ω - defines the location of the ascending and descending orbit locations with respect to the Earth's equatorial plane.
- ν - defines where the satellite is within the orbit with respect to perigee.

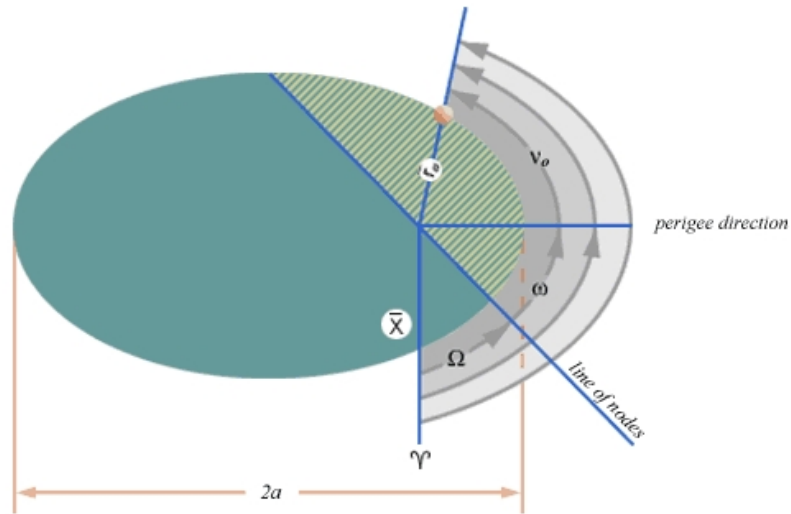


Figure 1.4. Orbital elements, courtesy Spaceflight.nasa.gov

1.5 Orbit Propagation

Orbit Propagation is the process of estimating the state of a celestial body at a given point of time, i.e, it is the process of obtaining the state as a function of time. In our case, it is the study of orbit of LAGEOS-II. The process of orbit propagation involves integration of the state variable to compute the state vector. Orbit propagation becomes complex when perturbations due to the central body (in our case Earth) are accounted for. As mentioned earlier we only consider the perturbations due to the non spherical shape of the Earth. We employ the Cowell's method for Orbit propagation which is explained as follows.

1.5.1 Cowell's Method

This method was developed by P.H.Cowell. This is the most simple and straightforward techniques of all the perturbation techniques. The technique deals with writing (1.12) as

$$\ddot{\mathbf{r}} + \frac{\mu}{r^3}\bar{\mathbf{r}} = \bar{\mathbf{g}}_p. \quad (1.14)$$

Bate [2] gives us the standard formulation for the Cowell's method in the Cartesian system as

$$\dot{\mathbf{r}} = \bar{\mathbf{V}}, \quad (1.15)$$

$$\dot{\mathbf{V}} = \bar{\mathbf{g}}_p - \frac{\mu}{r^3}\bar{\mathbf{r}}. \quad (1.16)$$

Hence the Cartesian components of (1.15) and (1.16) can be resolved as,

$$\dot{x} = V_x \quad \dot{V}_x = g_{px} - \frac{\mu}{r^3}x, \quad (1.17)$$

$$\dot{y} = V_y \quad \dot{V}_y = g_{py} - \frac{\mu}{r^3}y, \quad (1.18)$$

$$\dot{z} = V_z \quad \dot{V}_z = g_{pz} - \frac{\mu}{r^3}z, \quad (1.19)$$

where

$$r = \sqrt{x^2 + y^2 + z^2}. \quad (1.20)$$

Integrating equations (1.17) to (1.19) gives the Cartesian state vector. Also in order to integrate these equations, we need a set of initial conditions. Most of the satellite data which is available is used in the given TLE (Two Line Element) format. The TLE format contains the Keplerian elements corresponding to the ECI frame. Hence, they are converted to the Cartesian frame and then are integrated.

1.6 LAGEOS-II

In this research, we address the orbit of LAGEOS-II satellite. Hence, in this section we give a brief introduction to LAGEOS-II, which orbits at about 5781 km above Earth's surface. LAGEOS II satellite or the LASer GEOdetic Satellite is a highly dense (high mass-to-area ratio) laser retro-reflector satellite that provides a permanent reference point in a very stable orbit for precision geodetic studies. The satellite also provides a reference point for measurement of Earth rotation variations, solid Earth tides, and other kinematic and dynamic parameters associated with earthquake assessment and alleviation. This satellite is passive which means that it can only reflect the incident power. It consists of 426 reflectors designed to return a laser beam to the originating station. Of the 426 reflectors, which are also called as the cube corner retro-reflectors, 422 are made of fused silica and four of germanium. LAGEOS-II has a diameter of 60 cm and weighs about 405 Kg. Its compact and dense design facilitates its orbit to be precise. LAGEOS-II also permits extreme precision ranging measurements for both geometric mode and orbital dynamic mode determinations of positions of points on the Earth. The high-accuracy range measurements from LAGEOS-II's reference point are used to accomplish extreme precision Earth-dynamics measurements required by the earthquake hazard assessment and alleviation objectives of the Crustal Dynamics Project (CDP). The performance of LAGEOS II in orbit is only

limited by the degradation of the retro-reflectors, so many decades of useful life can be expected. IERS conventions[13] specify that a 20x20 spherical harmonic model is sufficient to describe the orbit of LAGEOS satellite.

1.7 GPS BIIA-10

A GPS satellite is a satellite used by the NAVSTAR Global Positioning System (GPS). The first satellite in the system, Navstar 1, was launched February 22, 1978. The GPS satellite constellation is operated by the 50th Space Wing of the United States Air Force. The construction of its orbits is made in a way such that the satellites do not concentrate near the poles. In this research we will also be addressing a GPS Block-IIA satellite, called the GPS BIIA-10. BIIA-10 has a mass of about 972.9 Kg and an orbital period of about 11 hours 59 minutes. The orbit of these satellites is at an altitude of about 20200 km. Hence, in this way it forms a good example for the Medium Earth Orbit (MEO). IERS conventions[13] specify that a 12x12 spherical harmonic model is sufficient to describe the orbit of GPS BIIA-10 satellite. Hence, we have defined the procedure for the orbit propagation technique that we will employ in for validating the MRQ Sphere model which will introduced in Chapter 3.

CHAPTER 2 SPHERICAL HARMONICS MODEL

The Spherical Harmonics Model is the conventional model for estimating the potential of a celestial object. It is commonly referred to as the ‘Standard Model’ or the ‘Reference Model’ and will here after in this literature will also be called as such. The Spherical Harmonics Model reference model uses ‘Legendre functions’ of the angular variables (latitudes and longitudes), upto a standard degree and order.

2.1 Description

In this chapter, we will use the reference model to estimate the state of the LAGEOS-II satellite. All the trajectories generated in this chapter are modeled using the reference model unless noted. We may develop algorithms written in MATLAB, python,C,C++ or any other computer language to run the simulation. We can use the Runge-Kutta Algorithm [5], as used by Jones[10].However, the MATLAB algorithm developed to evaluate these functions employs a Adams Bashforth-Moulton solver for the propagation for getting better accuracy and decreasing computation times. The integration tolerance used was of the order 10^{-20} and for a step length of 0.1 seconds.

2.2 Model Configuration

In this section be discuss the tools employed to configure the Spherical Harmonics Model. Gottlieb [7] gives the mathematical formulation for the potential function as

$$U = -\frac{\mu}{r} - \sum_{n=0}^{\infty} \sum_{m=0}^n \frac{\mu}{r} \left(\frac{R_e}{r}\right)^n P_{n,m}(\sin \phi) (C_{n,m} \cos(m\lambda) + S_{n,m} \sin(m\lambda)), \quad (2.1)$$

where μ is the gravitational parameter, R_e is the planetary radius, r is the magnitude, ϕ and λ are the latitudes and the longitudes of the position vector $X = (x_1, x_2, x_3)$ respectively,

$$P_{n,m}(\alpha) = (1 - \alpha^2)^{\frac{m}{2}} \left(\frac{\partial^m P_n}{\partial \alpha^m} \right) \quad (2.2)$$

are the associated Legendre functions, and P_n are the Legendre polynomials [7].

2.2.1 Gravity Coefficients

$C_{n,m}$ and $S_{n,m}$ are the un-normalized sine and cosine gravity coefficients, which are dependent on the mass distribution of the celestial body. These coefficients are generally published in their normalized form. The relation between these two forms is given by

$$\begin{aligned} C_{n,m} &= N(n, m) \bar{C}_{n,m} \\ S_{n,m} &= N(n, m) \bar{S}_{n,m} \end{aligned} \quad (2.3)$$

and

$$N(n, m) = \left(\frac{(n-m)!(2n+1)(2-\delta_{0m})}{(n+m)!} \right)^{\frac{1}{2}} \quad (2.4)$$

δ_{0m} is the delta function, i.e., $\delta_{0m} = 1$ if $m = 0$, otherwise $\delta_{0m} = 0$.

2.2.2 Derived Legendre Functions

The other important component in the traditional model formulation are the derived Legendre functions from eqn.2.2,

$$P_{n,m}(\alpha) = (1 - \alpha^2)^{\frac{m}{2}} P_n^m. \quad (2.5)$$

P_n^m are called the derived Legendre functions. We use one of the simpler recursive algorithm [7] to compute these functions which states

$$P_n^m = \frac{(2n-1)\alpha P_{n-1}^m - (n+m-1)P_{n-2}^m}{n-m}, (n > m), \quad (2.6)$$

$$P_n^n = (2n-1)P_{n-1}^{n-1}, \quad (2.7)$$

and $P_n^m = 0$ for $n < m$.

2.2.3 Formulation

Once the Legendre functions are computed, we can compute the potential using eqn.2.1. Then we can compute the acceleration vector inclusive of the perturbation as

$$\begin{aligned} \frac{\partial U}{\partial \bar{X}} = & -\frac{\mu}{r^2} \left(1 + \sum \sum \left(\frac{R_e}{r} \right)^n (n+m+1) \left(\frac{P_n^m B_{n,m}}{r^m} \right) \right) \frac{\bar{X}}{r} \\ & + \frac{\mu}{r^2} \sum \sum \left(\frac{R_e}{r} \right)^n P_n^{m+1} \frac{B_{n,m}}{r^m} \alpha - \frac{\mu}{r^2} \sum \sum \left(\frac{R_e}{r} \right)^n P_n^{m+1} \frac{B_{n,m}}{r^m} \frac{x_3}{r} \frac{\bar{X}}{r} \\ & + \frac{\mu}{r^2} \sum \sum \left(\frac{R_e}{r} \right)^n \frac{P_n^m}{r^{m-1}} \overline{D_{n,m}}. \end{aligned} \quad (2.8)$$

where,

$$B_{n,m} = (C_{n,m}\rho^m \cos(m\lambda) + S_{n,m}\rho^m \sin(m\lambda)). \quad (2.9)$$

$$\overline{D_{n,m}} = \begin{bmatrix} m(C_{n,m}\rho^{m-1} \cos((m-1)\lambda) + S_{n,m}\rho^{m-1} \sin((m-1)\lambda)) \\ -m(C_{n,m}\rho^{m-1} \sin((m-1)\lambda) + S_{n,m}\rho^{m-1} \cos((m-1)\lambda)) \\ 0 \end{bmatrix}, \quad (2.10)$$

$$\rho = \sqrt{x_1^2 + x_2^2}, \quad (2.11)$$

and

$$\alpha^T = \begin{bmatrix} 0 & 0 & 1 \end{bmatrix}. \quad (2.12)$$

For the exact formulation one might refer Gottlieb [7]. It is to be noted here that the acceleration computed with this formulation also includes the zero perturbation term, i.e.,

$$\frac{\partial U}{\partial \bar{X}} = \bar{g} + \bar{g}_p. \quad (2.13)$$

Once the perturbative acceleration vector is computed we can compute the position and velocity as mentioned earlier.

CHAPTER 3 MRQ-SPHERE MODEL

This chapter will be focused on configuring the MRQ Sphere model that was employed to compute the acceleration vector. The MRQ Sphere model was initially developed to estimate the gravity field of small bodies such as asteroids and comets. The model has been tested with asteroid EROS-433[10]

3.1 Introduction

The MRQ Sphere technique computes a multi-resolution representation of the gravity potential. The the angular variation functions are modeled by an alternate set of functions built using functions based on quadratures of a unit sphere that are invariant under the icosahedral group[1]. The construction of these quadratures uses a multi-resolution approximation to the Laplace's equation with the boundary values on the surface of a unit sphere. The individual terms have an exponential decay that accounts for a proper estimation of gravity functions at different distances. Localization of these polynomials is not provided here, and hence, we just state a concept that the spherical harmonics can be replaced by better localized functions. The shape of the central body is not focused in this study. Unlike the cubed-sphere gravity model, whose primary purpose is a fast evaluation of the gravity field [3], MRQ model is intended for estimation as it attempts to minimize the number of unknown parameters

The spherical harmonic modeling of irregularly shaped objects provides severe challenges and the difficulty increases with the complexity of the shape. Ellipsoidal Harmonics [6] has also proved accurate compared to spherical harmonics in the case of near ellipsoidal shaped asteroids like EROS-433. Therefore, other gravity representations for arbitrary shaped objects is always desired.

The MRQ-Sphere technique was able to reasonably approximate the gravity field of EROS, which was initially developed using the NEAR15A gravity model[11]. In this chapter, we intend to discuss the formulation and configuration of the Spherical Harmonics model and as a result look at the gravity estimation of LAGEOS-II satellite.

3.2 Formulation

The MRQ-Sphere employs two recently developed mathematical tools for formulating the multi-resolution representation of the gravity field. The first tool is used for approximating the radial decay using the sum of the Gaussians and the second tool is used for interpolation on a sphere for estimating the angular functions. We use these tools to compute the angular functions on each of these collection of spheres and use them to determine the potential. The approximation via gaussians also provides the separation of regions with different spatial resolutions. Instead of using the spherical harmonics we use functions generated by a single function by centering it at quadrature nodes with nearly even distribution on the sphere. The number of quadrature nodes increases with the increase in the degree of the gravity model. As mentioned earlier, the quadrature nodes are invariant under icosahedral group. These tools now constitute the multi-resolution model. The tools employed are discussed as follows.

3.2.1 Quadratures on the Sphere

The spherical harmonic model represents the gravitational field variations in the latitudinal and longitudinal directions using the standard global functions on the sphere. Hence, this quadrature based method has been developed [1] to

provide better localized functions. The nodes are constructed in such a way that they do not concentrate and have a near uniform distribution on the surface of a unit sphere. These nodes are also nearly optimal for a particular degree and order of the reference model. The combination is an analogue of the Lagrange type interpolation on the surface of the sphere. Now we introduce the technique developed by Ahrens and Beylkin [1] to introduce this section. As stated in eqn.2.1, the potential in the Spherical Harmonics domain is commonly expressed as

$$U(r, \phi, \lambda) = \frac{\mu}{r} \sum_{n=0}^{\infty} \left(\frac{R_e}{r} \right)^n \sum_{m=0}^n P_{n,m}[\sin \phi] (C_{n,m} \cos m\lambda + S_{n,m} \sin m\lambda), \quad (3.1)$$

where $P_{n,m}$ are the associated Legendre Polynomials. n is the degree, m is the order. ϕ is the longitude and λ is the latitude. $C_{n,m}$ and $S_{n,m}$ are the un-normalized cosine and sine gravity coefficients respectively. After representing the radius r in terms of planetary radius R_e ,

$$\rho = \frac{r}{R_e}. \quad (3.2)$$

We write the eqn.(3.1) as

$$U(r, \phi, \lambda) = \frac{\mu}{r} \sum_{n=0}^{\infty} \rho^{-(n+1)} V_n(\phi, \lambda). \quad (3.3)$$

Where,

$$V_n(\phi, \lambda) = \sum_{m=0}^n P_{n,m}[\sin \phi] (C_{n,m} \cos m\lambda + S_{n,m} \sin m\lambda). \quad (3.4)$$

Any function f in the space \mathcal{P}_N has the property

$$f(\alpha) = \int_{S^2} K_N(\alpha, \alpha') f(\alpha') d\alpha'. \quad (3.5)$$

Where K_N is the reproductive kernel given by

$$K_N(\alpha, \alpha') = \sum_{n=0}^N \frac{2n+1}{4\pi} P_{n,0}(\alpha, \alpha'), \quad (3.6)$$

and α and α' represent the unit vectors on the sphere S^2 . For a thorough discussion on the reproduction kernel, one can refer Arhens and Beylkin[1]. Having defined

the properties on a continuous domain, we now discretize equation (3.5) as follows,

$$f(\alpha) = \sum_{j=1}^M K_N(\alpha, \alpha_j) w_j f(\alpha_j). \quad (3.7)$$

Where M is the number of the quadrature nodes. $f(\alpha_j)$ are the values of the function on the nodes of these quadratures, and w_j are the weights of the nodes.

Of particular interest here are the number of nodes (M) needed in the eqn.(3.7) since the degree of the function under summation is $2N$. Hence, we choose the number of nodes needed to integrate the function of degree $2N$. This means that for a spherical harmonic model of degree n , we need M nodes which can optimally integrate functions of degree $2N$. Ahrens and Beylkin[1] have constructed these nodes to be invariant under the rotations of discrete icosahedral group.

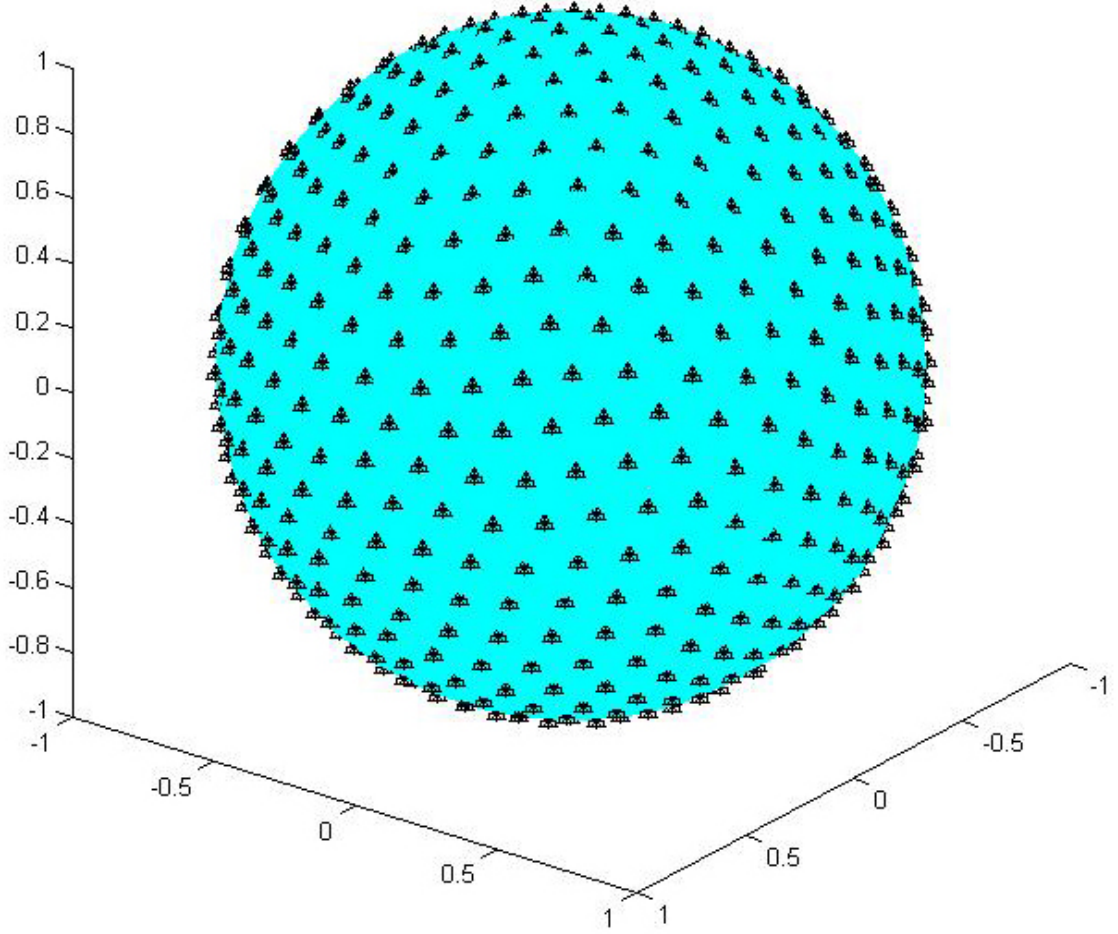


Figure 3.1. Nodes used for the orbit propagation. ($2N = 40, M = 612$)

Since the orbit of study can be well explained by a 20x20 Spherical harmonic model as suggested by IERS 2010 conventions [13], we use the number of nodes to integrate a function of degree 40 due to the reason stated above. These nodes are shown graphically on a unit sphere in fig.3.1. The reproducing Kernel in the (3.6) can be interpreted using the Christoffel-Darboux formula [14] as

$$K_N(\gamma) = \frac{N+1}{4\pi} \left(\frac{P_{N,0}(\gamma) - P_{N+1,0}(\gamma)}{1-\gamma} \right). \quad (3.8)$$

Then according to Szegő[14] eq. (3.8) becomes

$$K_N(\gamma) = \frac{N+1}{4\pi} P_N^{(1,0)}(\gamma). \quad (3.9)$$

Where $P_N^{(1,0)}$ is the the Jacobi polynomial with $\alpha = 1$ and $\beta = 0$. Therefore, to avoid confusion of Jacobi polynomials $P_N^{(1,0)}$ with the Legendre Polynomials P_N , we define

$$\bar{K}_N(\gamma) = \frac{4\pi}{N+1} K_N(\gamma) = P_N^{(1,0)}(\gamma). \quad (3.10)$$

Then following the recursive formulation of the jacobian polynomial[8], we get

$$\bar{K}_N(\gamma) = \left(c_1 \gamma + \frac{1}{c_0} \right) \bar{K}_{N-1}(\gamma) - (c_2) \bar{K}_{N-2}(\gamma). \quad (3.11)$$

Where

$$\bar{K}_0(\gamma) = 1, \quad (3.12)$$

$$\bar{K}_1(\gamma) = \frac{3\gamma + 1}{2}, \quad (3.13)$$

and,

$$c_0 = (n+1)(2n-1), \quad (3.14)$$

$$c_1 = \frac{(2n-1)(2n+1)}{c_0} = \frac{(2n+1)}{(n+1)}, \quad (3.15)$$

$$c_2 = \frac{(n-1)(2n+1)}{c_0}. \quad (3.16)$$

We also define

$$\frac{\partial \bar{K}_N(\gamma)}{\partial \gamma} = c_1 \bar{K}_{N-1}(\gamma) + \left(c_1 \gamma + \frac{1}{c_0} \right) \frac{\partial \bar{K}_{N-1}(\gamma)}{\partial \gamma} - c_2 \frac{\partial \bar{K}_{N-2}(\gamma)}{\partial \gamma} \quad (3.17)$$

where

$$\frac{\partial \bar{K}_0(\gamma)}{\partial \gamma} = 0, \quad (3.18)$$

$$\frac{\partial \bar{K}_1(\gamma)}{\partial \gamma} = \frac{3}{2}, \quad (3.19)$$

and

$$\frac{\partial \bar{K}_N(\gamma)}{\partial \gamma} = \frac{N+1}{4\pi} \frac{\partial K_N(\gamma)}{\partial \gamma}. \quad (3.20)$$

The partials of these Kernels is computed in order to find the acceleration vector. In order to understand the behavior of the Kernel and its derivative response of both the functions is shown in fig.3.2. Therefore in this manner, the Reproductive Kernel is computed by means of the Jacobi Polynomial.

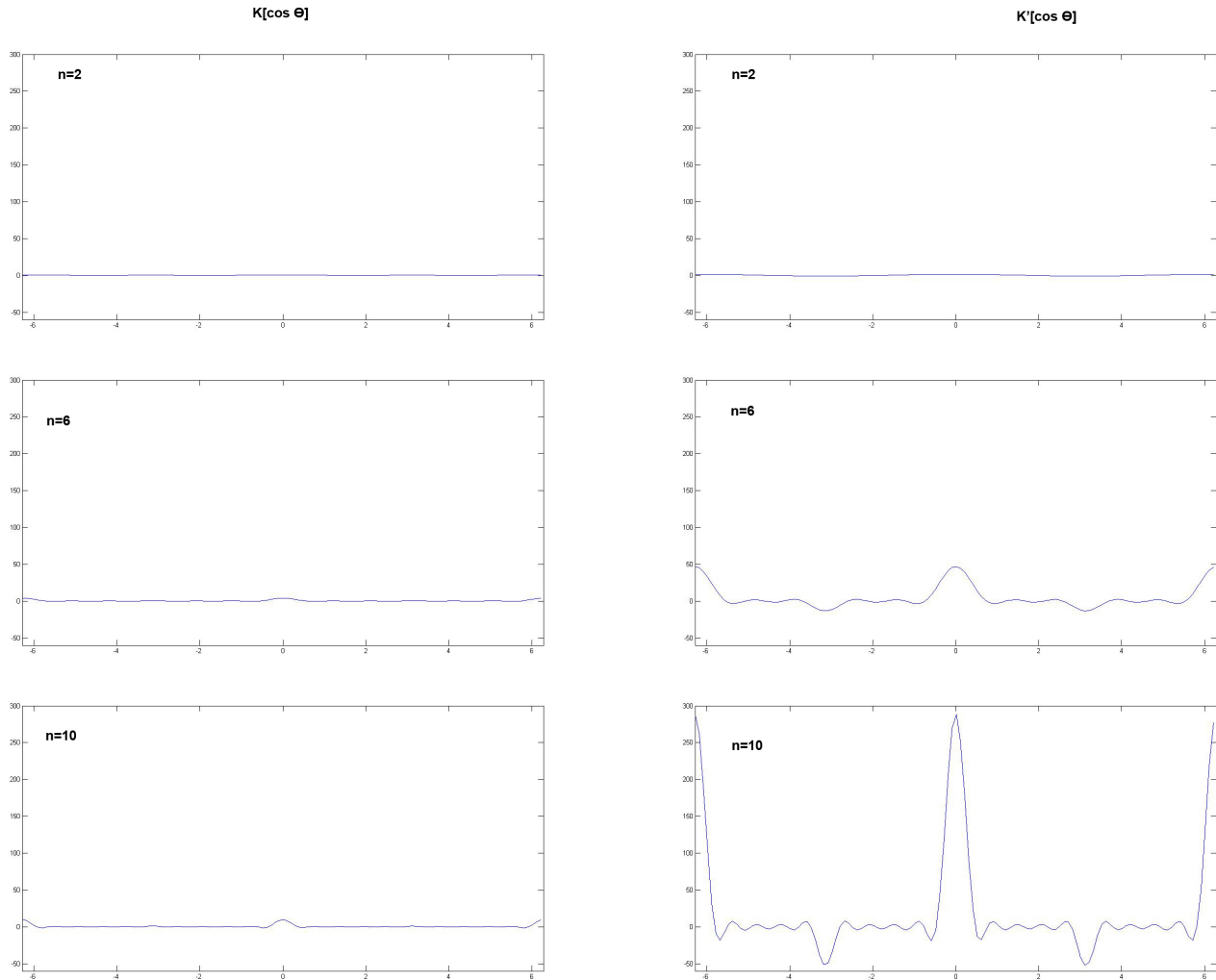


Figure 3.2. Plots of the Kernel matrix and its partial derivative as a function of angle between the two unit vectors

3.2.2 Approximation by Gaussians

As mentioned earlier, radial decay is approximated by using the Gaussians. Beylkin and Monzón [4] state that for a user defined precision $\epsilon > 0$ there exists a Gaussian step size h and a positive M such that

$$|e^{-xy} - G_{h,M}(x, y)| \leq \epsilon. \quad (3.21)$$

Where $G_{h,M}$ represents the Gaussian approximation computed as predicted by (1.7)

$$G_{h,M} = \frac{hx}{\sqrt{4\pi}} \sum_{j=0}^M e^{\left(-\frac{x^2}{4}e^{s_j} - y^2e^{-s_j} + \frac{s_j}{2}\right)} \quad (3.22)$$

and

$$s_j = s_{start} + jh. \quad (3.23)$$

Following the derivation by Jones[10], we write the radial decay approximated by the Gaussians as

$$\rho^{-(n+1)} \approx G_{h,Z}(n+1, \ln \rho) = \frac{hx}{\sqrt{4\pi}} \sum_{j \in \mathcal{Z}} \frac{1}{\left(\sigma_j e^{\left(\frac{n+1}{2\sigma_j}\right)^2} e^{\frac{(\sigma_j \log \rho)^2}{2}}\right)} \quad (3.24)$$

where

$$\sigma_j = \sqrt{2e^{jh}}. \quad (3.25)$$

Hence now, we can define the MRQ potential as

$$U(\rho, \phi, \theta) = \frac{\mu}{r} \sum_{j \in \mathcal{Z}} e^{-\frac{(\sigma_j \ln \rho)^2}{2}} Z_j(\phi, \theta), \quad (3.26)$$

where

$$Z_j(\phi, \theta) = \frac{h}{\sigma_j \sqrt{2\pi}} \sum_{n=0}^{\infty} (n+1) e^{-\left(\frac{n+1}{2\sigma_j}\right)^2} V_n(\phi, \theta). \quad (3.27)$$

Where $V_n(\phi, \theta)$ is given by (3.4). One must not mistake the \mathcal{Z} in the summations (3.26) and (3.24) with the Z_j functions as the \mathcal{Z} in the summation represents the set of integers.

3.3 Model

Now as we have briefed tools employed by the MRQ-Sphere model in this section we will discuss the formulation of the model for both potential and acceleration.

3.3.1 Potential Function

As it can easily be observed that the terms in the potential function decay exponentially with increasing degree and order, we can limit the number of summation terms j such that $j \in \mathcal{J}$ where $\mathcal{J} \subset \mathcal{Z}$. Following Arhens and Beylkin [1], we write (3.26) as

$$U(\rho, \phi, \theta) = \frac{\mu}{r} \sum_{j \in \mathcal{J}} e^{-\frac{(\sigma_j \ln \rho)^2}{2}} Z_j(\phi, \theta), \quad (3.28)$$

and the functions $Z_j(\alpha)$ can be estimated by using from the points on the Quadrature nodes of the MRQ sphere as

$$Z_j(\alpha) = \sum_{i=1}^M K_N(\alpha, \alpha_i) w_i Z_j(\alpha_i). \quad (3.29)$$

α_i represent the quadrature nodes while M denotes the number of nodes.

3.3.2 Acceleration Vector

Following Jones[10], we have the acceleration given by the MRQ sphere as

$$\bar{g} = \frac{\mu}{r} \sum_{j \in \mathcal{J}} e^{-(\sigma_j \ln \rho)^2/2} \left[\left(-\frac{\sigma_j^2}{r^2} (\ln \rho) Z_j(\hat{r}) \right) r + \left(\frac{\partial \hat{r}}{\partial r} \right) \left(\sum_{l=1}^M w_l Z_j(\alpha_l) \frac{\partial K_n(\gamma)}{\partial \gamma} \right) \alpha_l \right], \quad (3.30)$$

where

$$\frac{\partial \hat{r}}{\partial r} = \frac{I_{3 \times 3}}{r} - \frac{r r^T}{r^3}. \quad (3.31)$$

Missions to bodies beyond Earth employ a Square Root Information Filter (SRIF) which can estimate the position of satellite, gravity field, and other parameters which can generate an initial low degree reference model. Tsoulis[17] describes

how to generate this low degree spherical harmonics model. We then estimate Z_j functions using the least squares algorithm[15]. However in our model we use (3.27) and (3.4) to compute the Z_j function.

3.4 Model Configuration

Now that all the functions that are used in the computation of the acceleration have been introduced, we focus on configuring this model as we have done in the propagation tests. Initially, we select a user-desired precision ϵ for the problem at hand which has a fixed degree and order. In our case LAGEOS-II satellite is a 20x20 spherical Harmonic model. Then for the given ϵ , we compute an initial Gaussian step size as,

$$h_0 = \frac{1}{\beta_1 + \beta_2 \log_{10} \epsilon^{-1}} \quad (3.32)$$

where

$$\beta_1 = 0.0983589778057344, \quad (3.33)$$

$$\beta_2 = 0.234434655957678. \quad (3.34)$$

These values are taken from a non-linear curve fitting problem resulting from various observations taken from Jones [10] as shown in 3.1.

Table 3.1. Data points used for computing initial Gaussian stepsize, Jones [10].

h	ϵ	h	ϵ
0.9	4.95×10^{-5}	0.5	7.65×10^{-9}
0.8	1.23×10^{-5}	0.4	5.5×10^{-11}
0.7	2.11×10^{-6}	0.3	1.64×10^{-14}
0.9	2.00×10^{-7}		

We then select the subset $j \in \mathcal{J}$, referred to as shells from here after, that will satisfy the user-defined precision. Hence based on the radius of orbit in terms of the radius of the central body, we can configure the number of shells.

Table 3.2. Data points used for computing initial Gaussian stepsize, Jones[10].

Range ρ	j_{min}	j_{max}
Above 33.963085	-5	0
33.963085-17.221399	-5	1
17.221399-10.223156	-5	2
10.223156-6.437202	-5	3
6.437202-4.578281	-5	4
4.578281-3.412891	-5	5
3.412891-2.702480	-5	6
2.702480-2.244688	-5	7
2.244688-1.925941	-5	8

Table 3.2 shows the range of values used by Jones [10] in configuring MRQ Sphere model for the asteroid EROS-433 where the initial Gaussian (h_0) step size was 0.425. The algorithm in computing the shells is to start with an initial shell Gaussian step size and increase the number of shells until we reach the required accuracy. Then we improvise the Gaussian step size. It can be observed from the table 3.2 that the number of shells increase with a decrease in the radius.

In this research of configuring the MRQ sphere model for LAGEOS-II satellite, the radius range varies from 1.93238561854188-1.87990245591832, so we use the shells ranging from $j=-13$ to $j=12$.

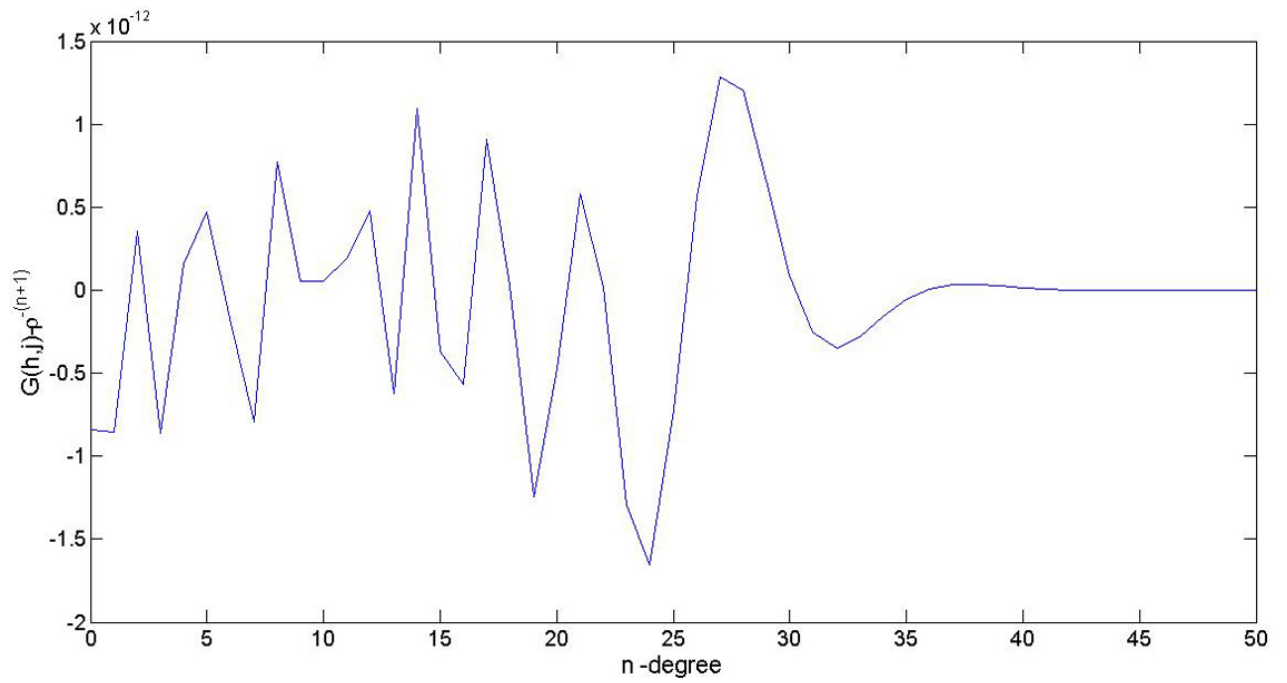


Figure 3.3. Error between the radial decay and the gaussian approximation for $j_{min} = -13$, $j_{max} = 12$, $h = 0.3435$, and $\rho = \rho_{min} = 1.8799$.

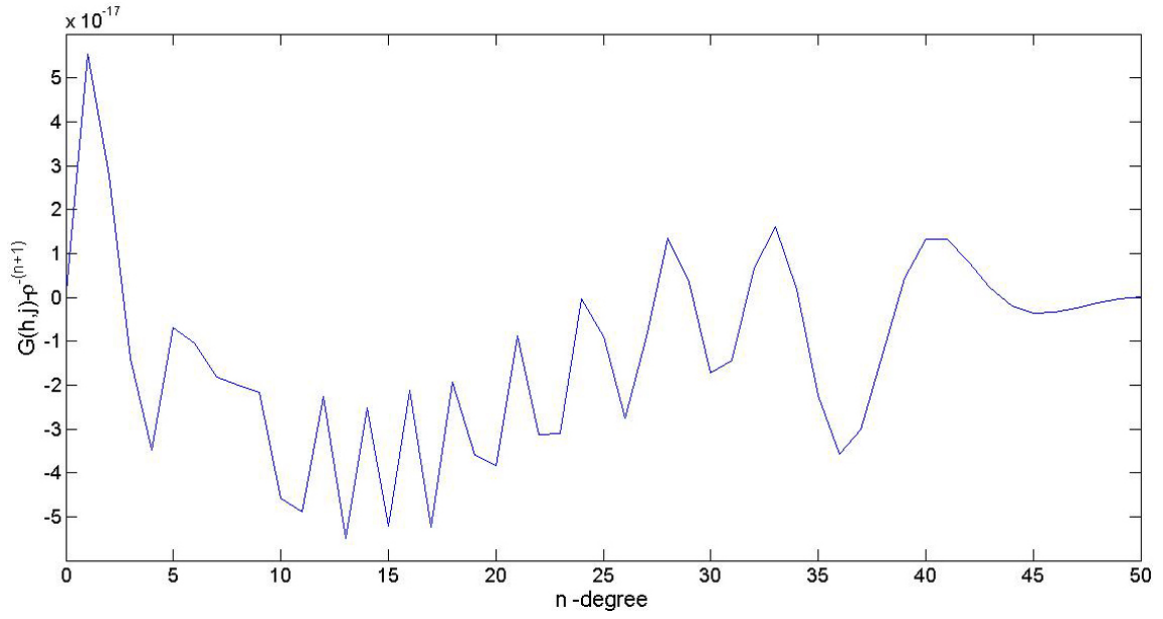


Figure 3.4. Error between the radial decay and the gaussian approximation for $j_{min} = -20$, $j_{max} = 17$, $h = 0.2487$, and $\rho = \rho_{min} = 1.8799$.

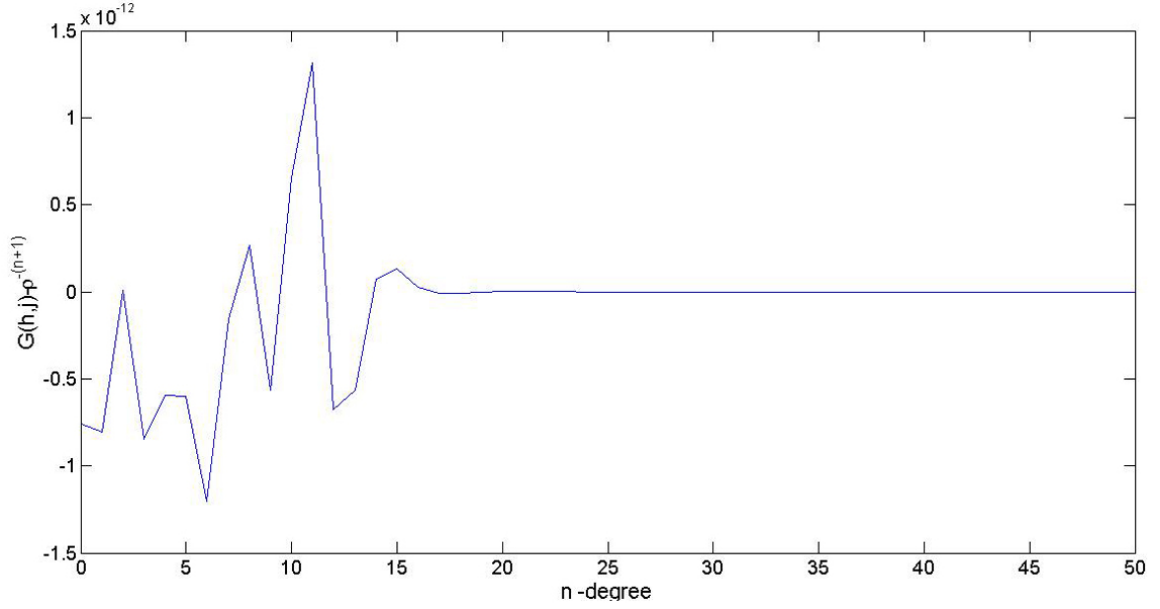


Figure 3.5. Error between the radial decay and the gaussian approximation for $j_{min} = -13$, $j_{max} = 7$, $h = 0.3465$, and $\rho = \rho_{min} = 4.1141$.

One can always check the validity of configuration of h and j by plotting the error between the Gaussian and the radial function and see if it falls in our accuracy region, i.e.,

$$|G(h, j) - \rho^{-(n+1)}| < \epsilon \quad (3.35)$$

Figures 3.3, 3.4, and 3.5 show the configuration check used in the case of this research. Since our accuracy was around 4×10^{-12} , we were well within the accurate region. The Gaussian step size and the desired accuracy together constitute the MRQ Sphere gravity model which is the equivalent of a spherical harmonics model whose degree and order are known. We also present the configuration of the model for improved accuracy at $\epsilon=9 \times 10^{-17}$ and also for the GPS satellite where we choose an accuracy of $\epsilon=4 \times 10^{-12}$.

Table 3.3. Configuration for the MRQ sphere model representation of LAGEOS-II.

Attribute	Value
Satellite	Lageos-II
Degree and Order	20x20
Gaussian Step size	0.3435(Test-I)
Gaussian Step size	0.2487(Test-II)
Precision ϵ of approximating $\rho^{-(n+1)}$	4×10^{-12} (Test-I)
Precision ϵ of approximating $\rho^{-(n+1)}$	9×10^{-17} (Test-II)
Number of Nodes α_i	612

Table 3.4. Configuration for the MRQ sphere model representation of GPS BIIA-10.

Attribute	Value
Satellite	GPS BIIA-10 (PRN 32)
Degree and Order	12x12
Gaussian Step size	0.3465(Test-I)
Precision ϵ of approximating $\rho^{-(n+1)}$	4×10^{-12}
Number of Nodes α_i	372

Hence to summarize the configuration of the MRQ-Sphere model, tables 3.3 and 3.4 represents the parameters that were used to configure the MRQ sphere model that was employed in this research.

CHAPTER 4 RESULTS

This chapter we test the validity of the MRQ-Sphere model against the traditional spherical harmonics in terms of orbit Propagation. As discussed earlier we perform the tests for a for a maximum radial accuracy of $\epsilon_{max} = 4 \times 10^{-12}$. The results of the tests are presented below as follows. Configurations used in this research are shown in tables 3.3 and 3.4. The module was initially computed and checked for its gravitational accuracy. We find that gravity anomalies do exist, and also they are maximum at the extreme end of the asteroid when compared to the Spherical Harmonic Model [12]

4.1 Gravity Estimation

This Model chosen was to approximate a 20 x 20 spherical harmonics of LAGEOS-II model with the number of nodes to approximate a function of degree 40 x 40. The MRQ Sphere gravity vector was computed according to the eqn.(3.30) and a reference gravity vector, i.e, the eqn.(2.8) and their norms were compared as shown in Fig.4.1

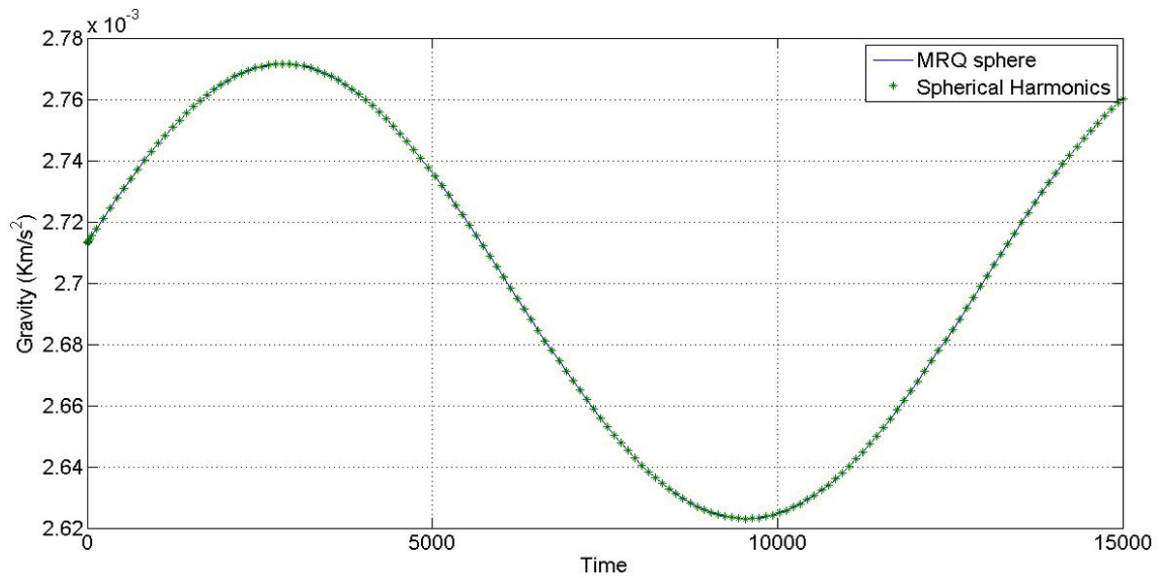


Figure 4.1. Gravity as predicted by spherical harmonics and the MRQ Sphere model.

The response shows that the computed MRQ-sphere gravity vector does agree with the reference Spherical Harmonics model. The peaks of the plot are at the perigee and apogee of the orbit trajectory. The error computed between the two plots is shown in Fig.4.2.

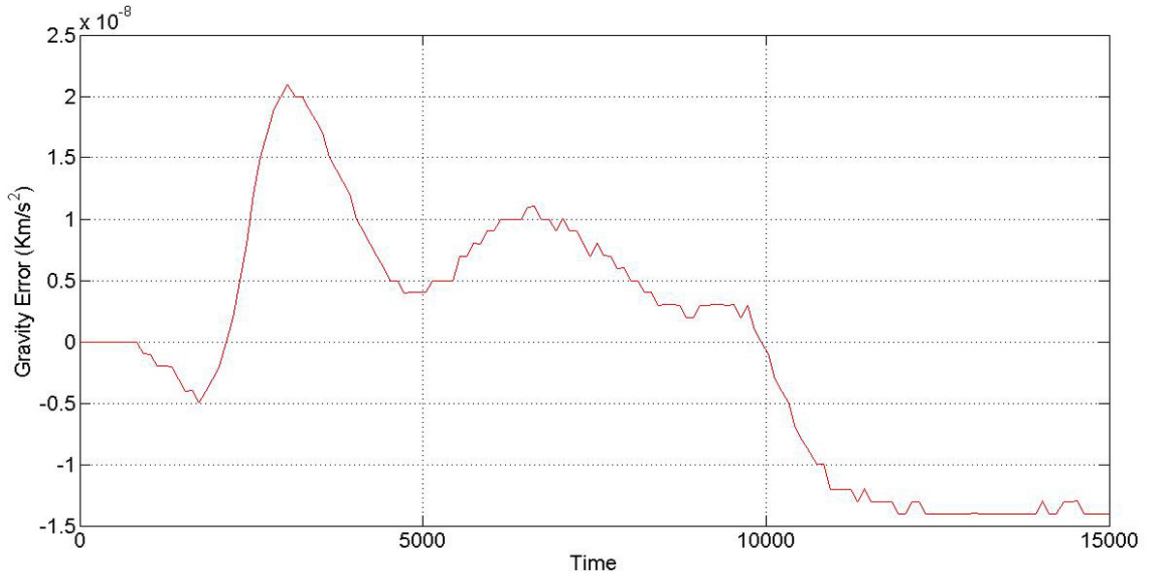


Figure 4.2. Error response of the MRQ sphere acceleration gravity as compared to the Spherical Harmonics gravity.

The computed error is of the order 4×10^{-8} , which is within the accepted accuracy range. Hence, we verify the accuracy of the model for the gravity and proceed to the orbit propagation comparison responses.

4.2 Orbit Propagation Results

Tests were conducted to compute both the Keplerian elements and the Cartesian components and are presented below.

4.2.1 Keplerian Elements

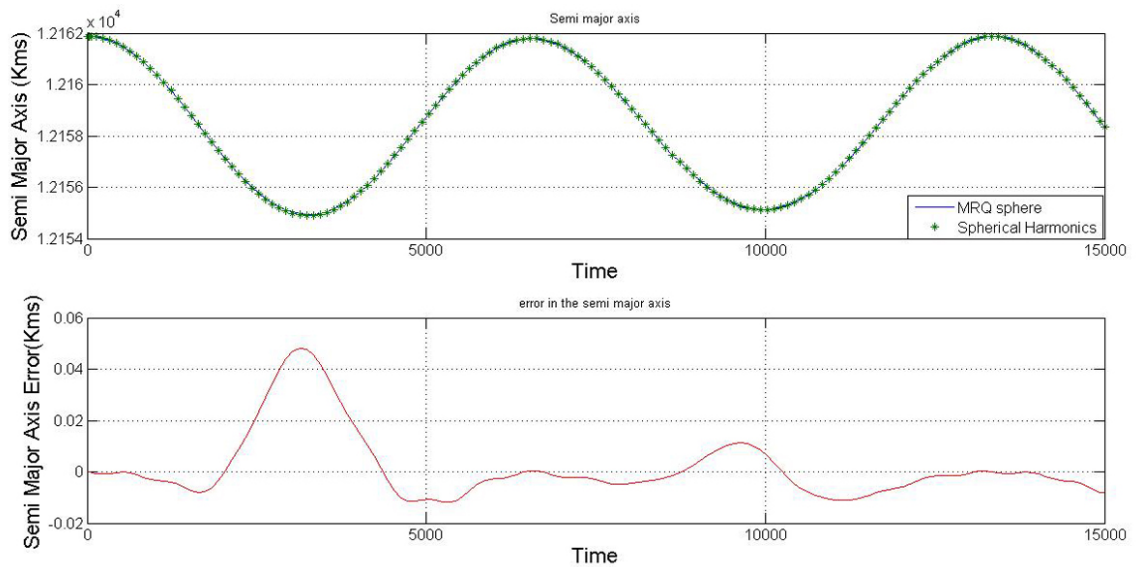


Figure 4.3. Plot showing the variation of semi major axis as predicted by the MRQ Sphere model and Spherical harmonics and the error between the two models.

Fig. 4.3 shows the variation of the semi major axis as approximated by the MRQ-sphere and as predicted by the spherical harmonics model. The error response shows a variation of about 0.04 Kms.

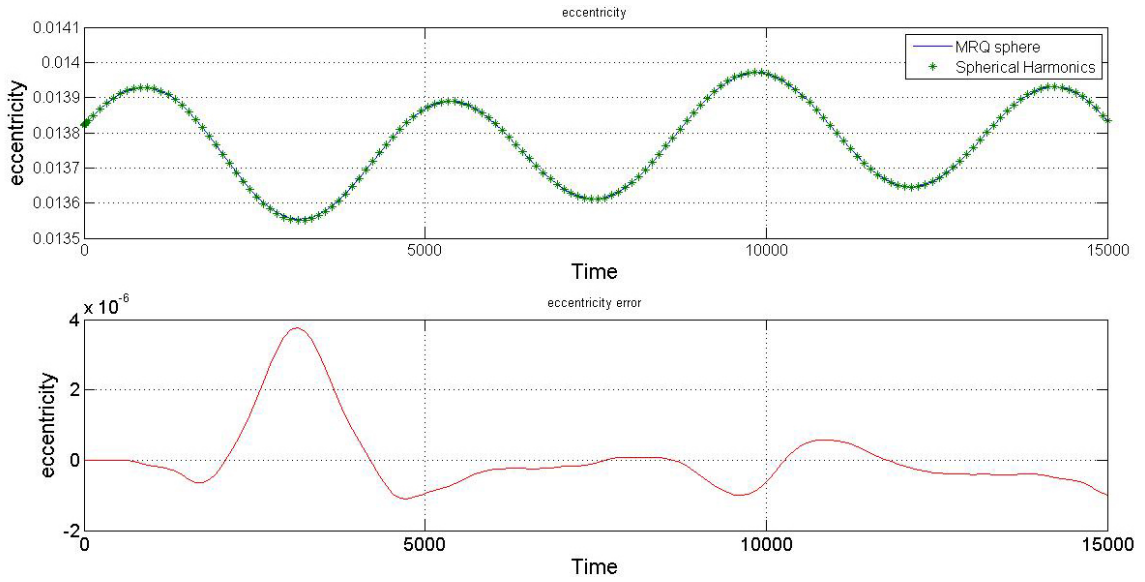


Figure 4.4. Plot showing the variation of eccentricity as predicted by the MRQ Sphere model and Spherical harmonics and the error between the two models.

Fig. 4.4 shows the eccentricity response of the two models, and the error between the MRQ sphere model and the spherical harmonics model, and the deviation is of order 4×10^{-6} ; however, the behavior of the eccentricity agrees with with the spherical harmonics.

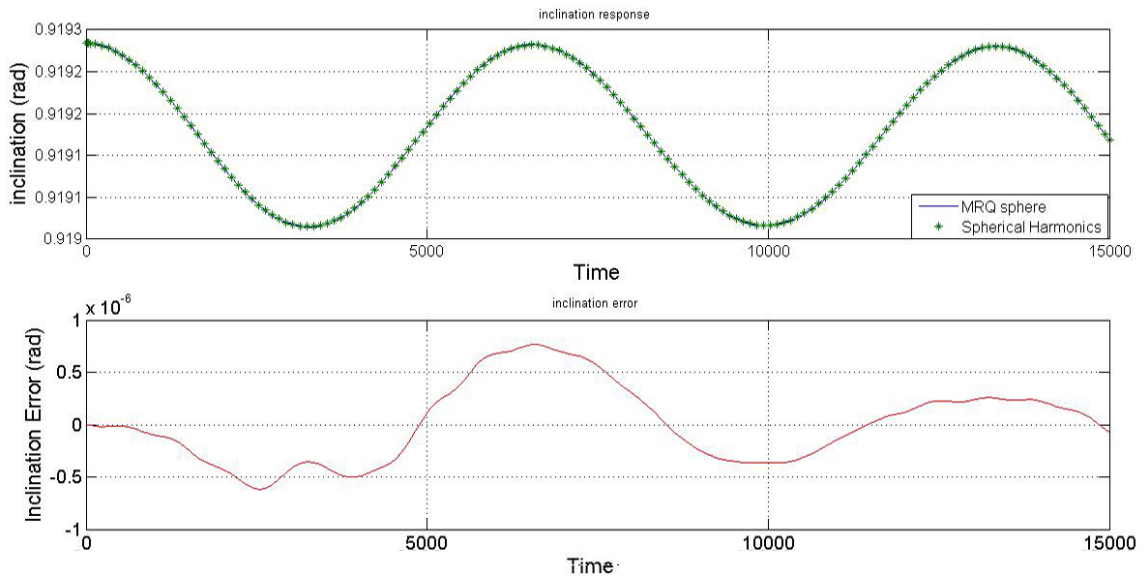


Figure 4.5. Plot showing the variation of inclination as predicted by the MRQ Sphere model and Spherical harmonics and the error between the two models.

Fig.4.5 shows the response of the inclination of the orbit with respect to time as approximated by the MRQ sphere model and the spherical harmonics model. The responses do agree with each other, and the error is of the order of 10^{-7} radians.

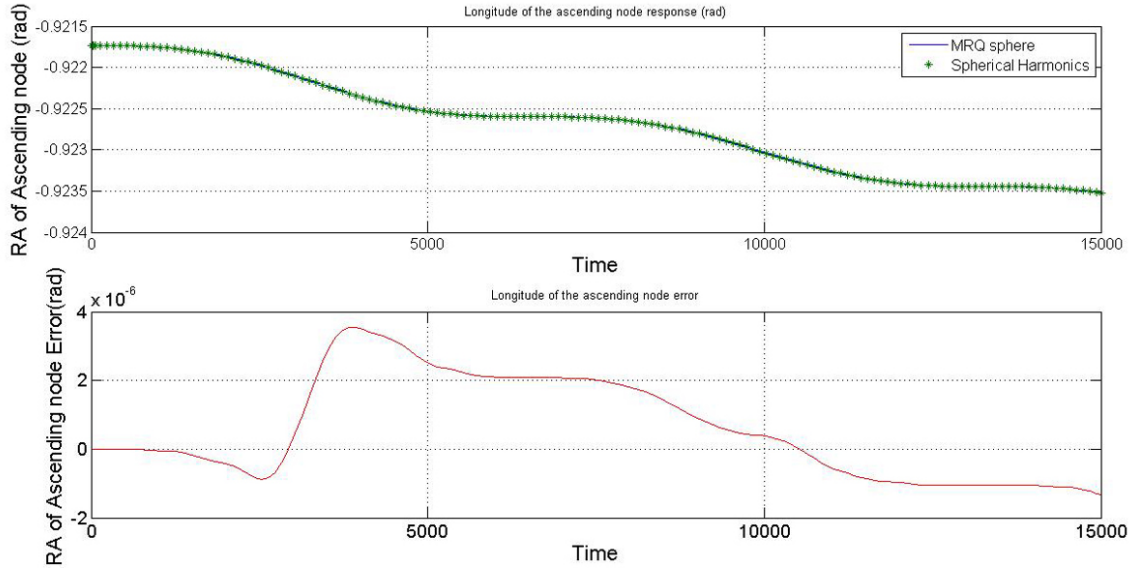


Figure 4.6. Plot showing the variation of longitude of the ascending node as predicted by the MRQ Sphere model and Spherical harmonics and the error between the two models.

Fig. 4.6 shows the response of the longitude of the ascending node with respect to time as approximated by the MRQ sphere model and the spherical harmonics model. The responses do agree with each other, and the error is small.

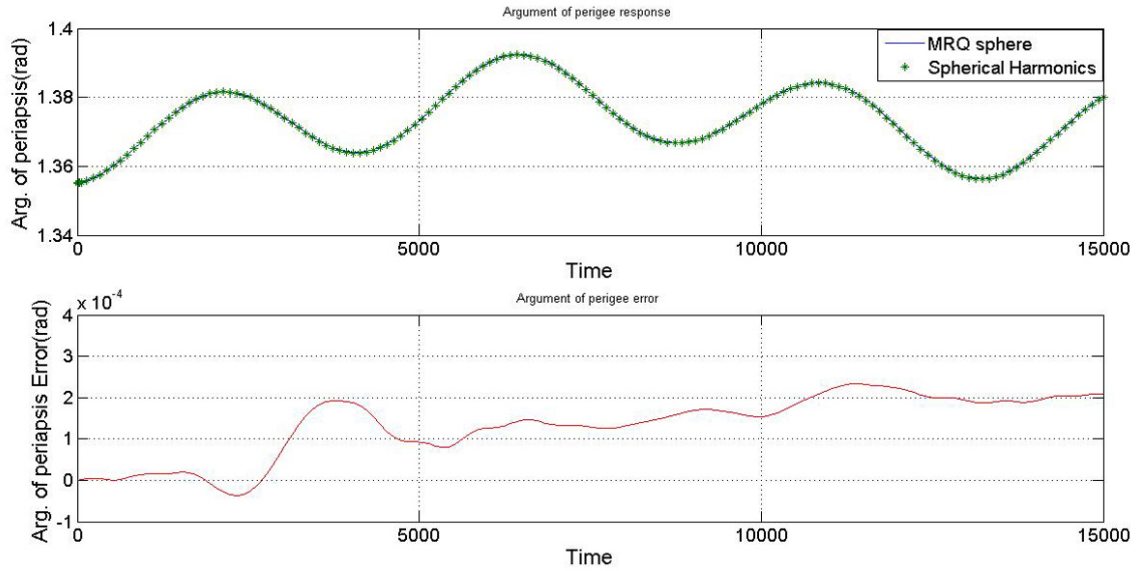


Figure 4.7. Plot showing the variation of argument of perigee as predicted by the MRQ Sphere model and Spherical harmonics and the error between the two models.

Fig.4.7 shows the response of the argument of perigee with respect to time as approximated by the MRQ sphere model and the spherical harmonics model. The responses do agree with each other, and the error is small.

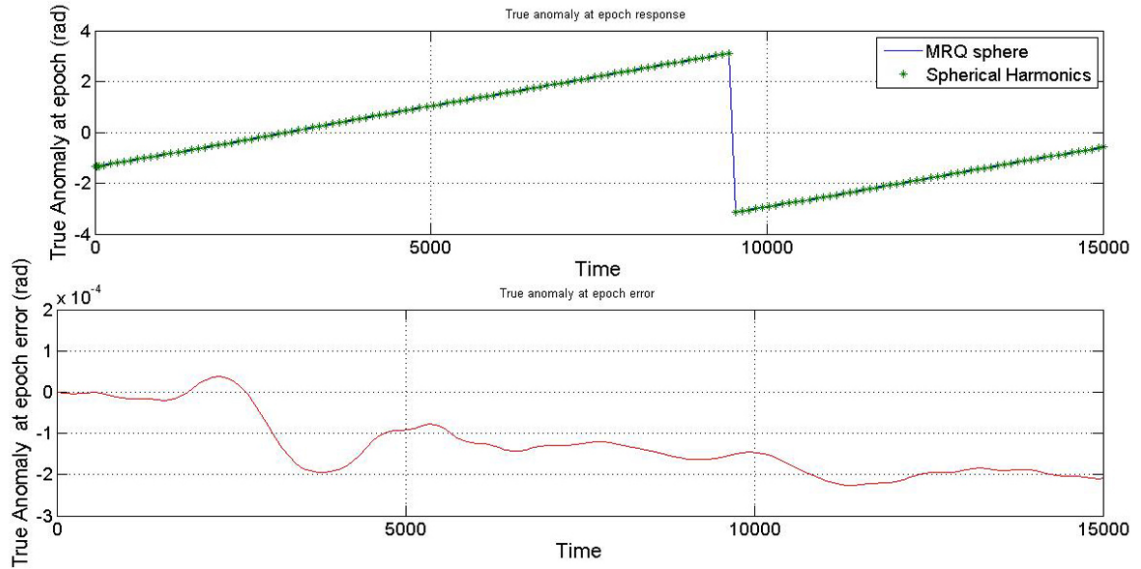


Figure 4.8. Plot showing the variation of true anomaly at epoch as predicted by the MRQ Sphere model and Spherical harmonics and the error between the two models.

Fig.4.8 shows the response of the true anomaly at epoch with respect to time as approximated by the MRQ sphere model and the spherical harmonics model. The responses follow the same response with a maximum error of about 2×10^{-4} radians which is considered small.

4.2.2 Cartesian Variation

Having presented the variation of Keplerian elements, we now move ahead to compare the Cartesian formulation.

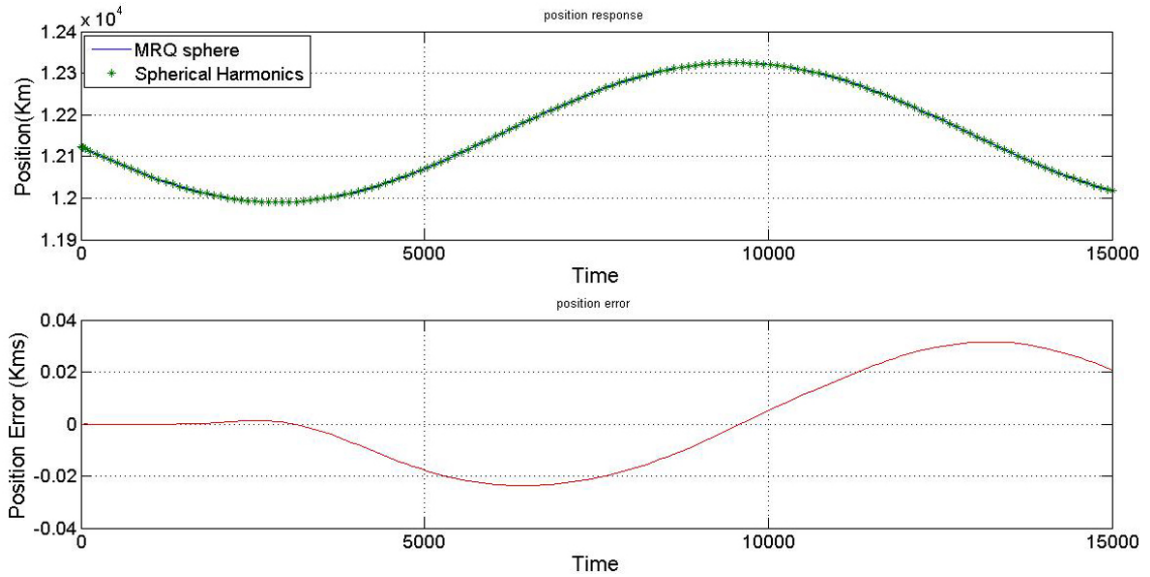


Figure 4.9. Plot showing the variation position response as predicted by the MRQ Sphere model and Spherical harmonics and the error between the two models.

Fig.4.9 shows the response of the position of the satellite with respect to time as approximated by the MRQ sphere model and the spherical harmonics model. The response follows the same trend; however, the baseline for comparison is in kilometers. Hence the error between the responses of 0.04 km is a subject to the matter of user accuracy.

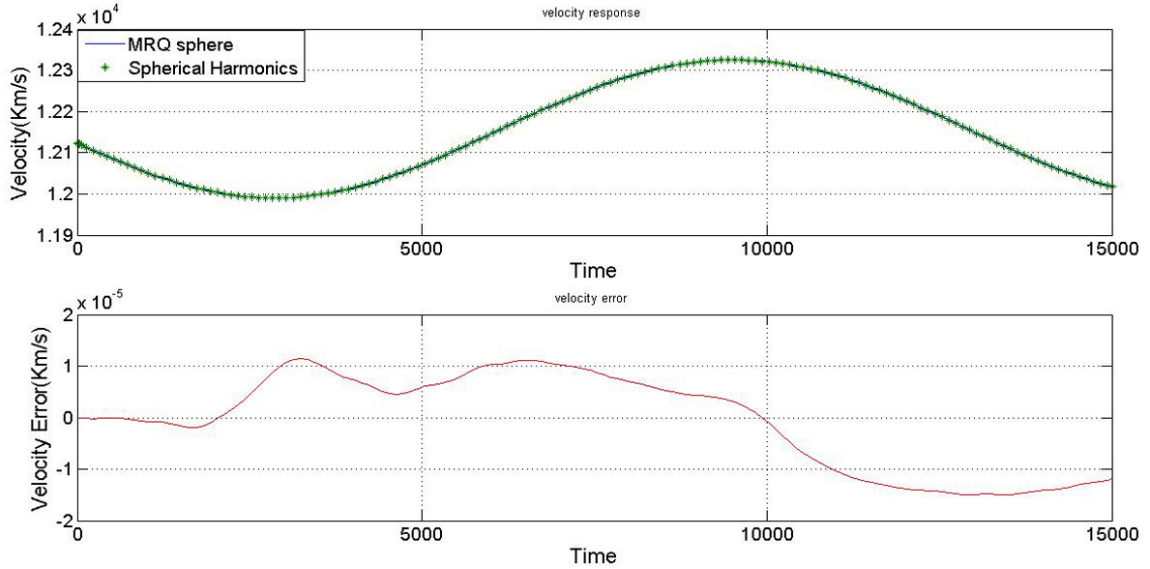


Figure 4.10. Plot showing the variation position response as predicted by the MRQ Sphere model and Spherical harmonics and the error between the two models.

Fig.4.10 shows the response of the velocity of the satellite with respect to time as approximated by the MRQ sphere model and the spherical harmonics model. The responses have the same trend. We encounter an error of the order 10^{-5} Km/s, which is very low.

4.2.3 Impact of the Number of Shells

In order to investigate the impact of the number of shells on the orbit propagation, we vary the number of shells in the MRQ-sphere model. We verify that after reaching the optimal number of shells any increase will not effect the parameters. Also, we find that a decrease in the number of shells leads to vast difference in the results as indicated by figures 4.11 and 4.12.

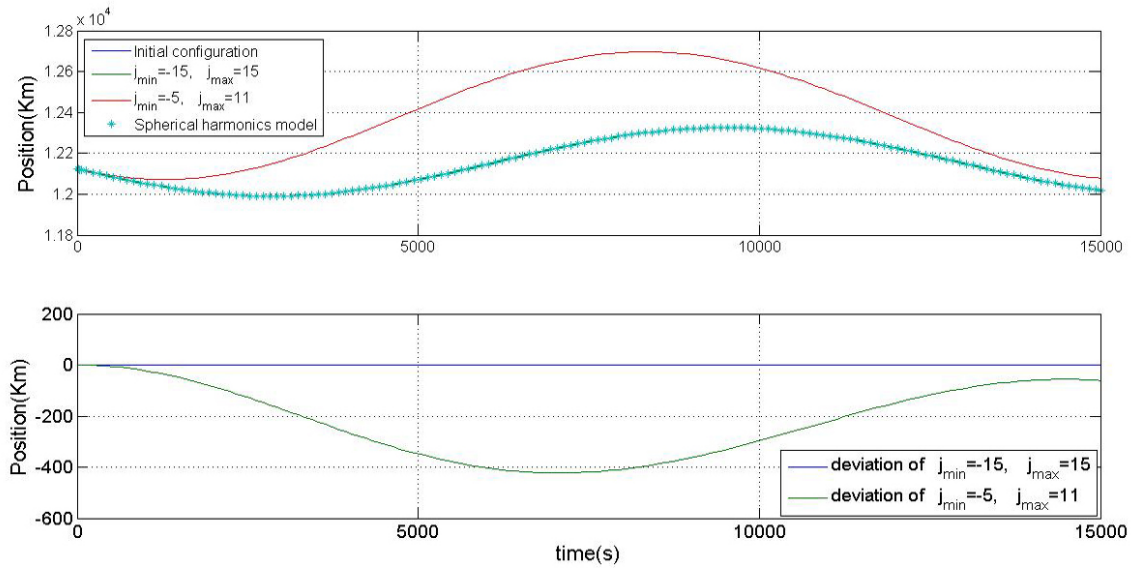


Figure 4.11. Plot showing impact of number of shells on the position of the satellite predicted by the model.

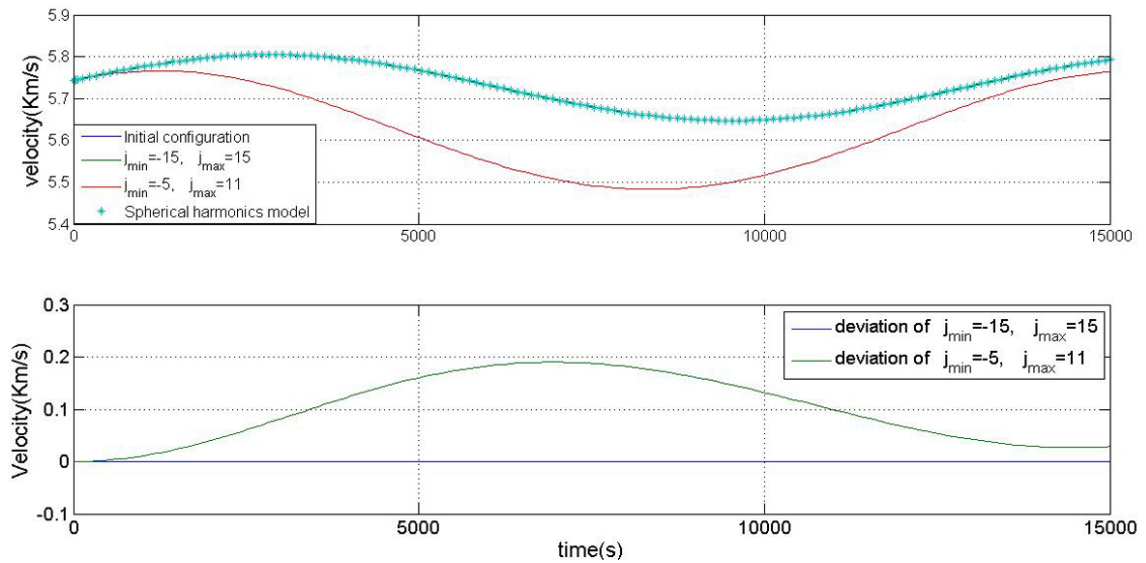


Figure 4.12. Plot showing impact of number of shells on the velocity predicted by the model.

4.2.4 Impact of the Radial Decay Accuracy

We also try to increase the radial decay term accuracy to about 9×10^{-17} at a Gaussian step size of 0.248702046384601, but there is no significant impact on the parameters as shown in figures 4.13, 4.14, and 4.15.

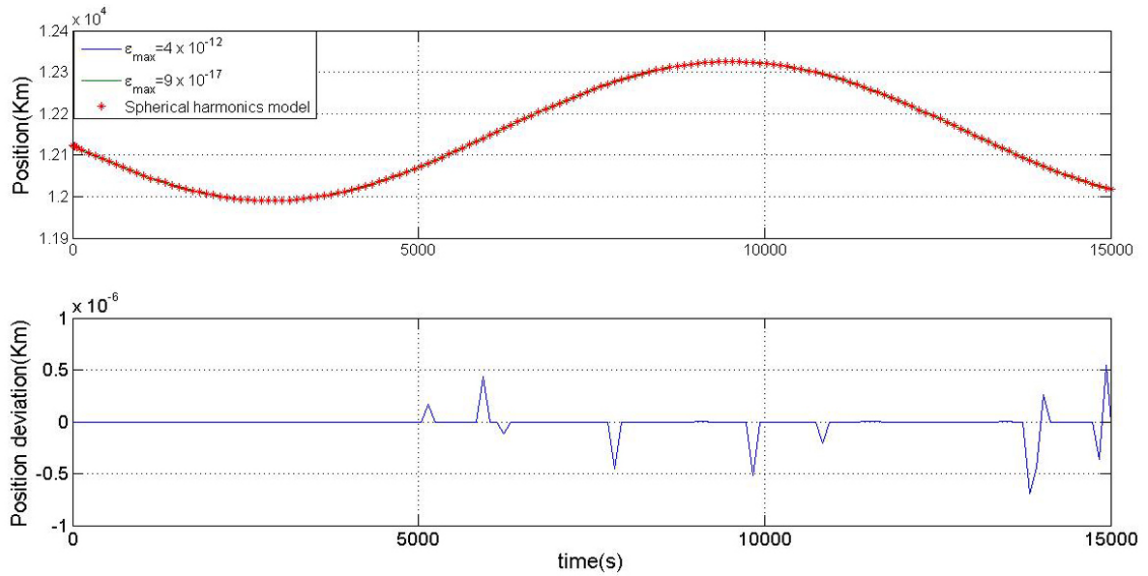


Figure 4.13. Plot showing impact of radial accuracy on the position of the satellite predicted by the model.

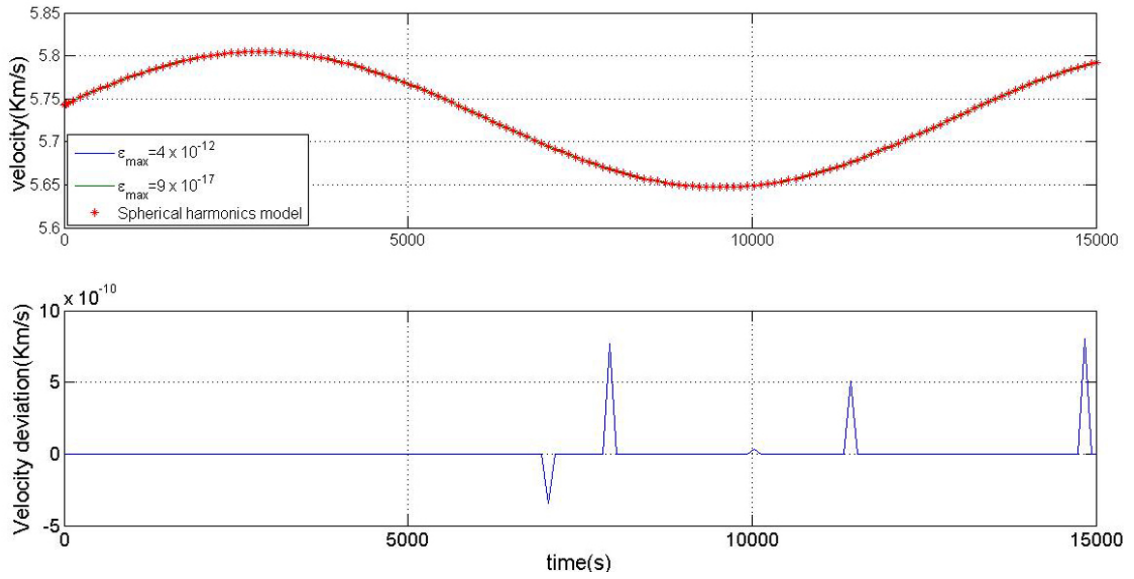


Figure 4.14. Plot showing impact of radial accuracy on the velocity predicted by the model.

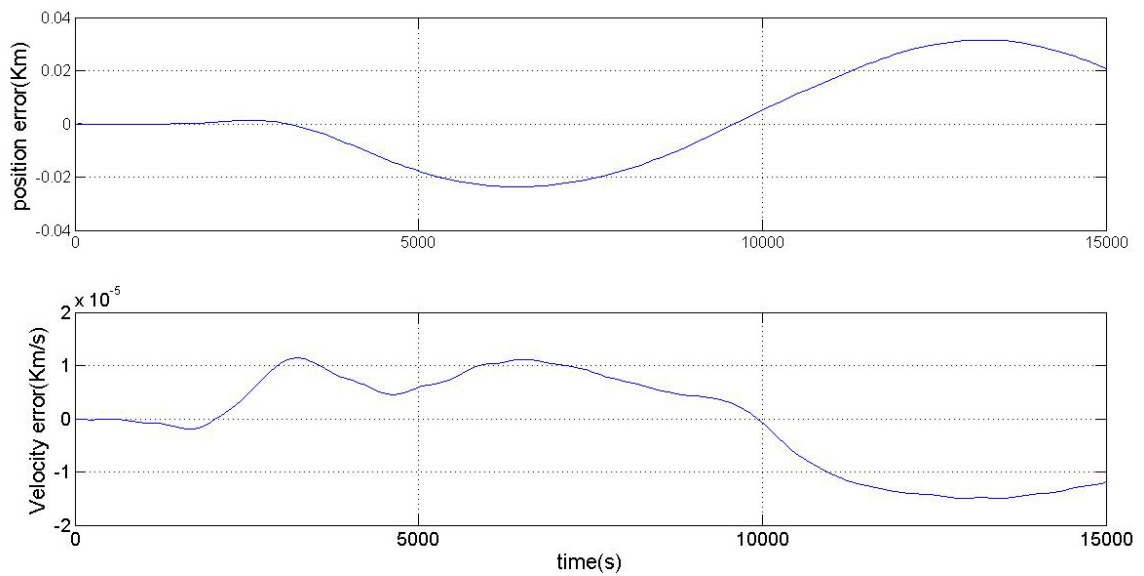


Figure 4.15. Plot showing error in position and velocity of LAGEOS-II between the accuracy improved MRQ sphere model and the spherical harmonics.

4.3 GPS BIIA-10 Results

4.3.1 Gravity Vector

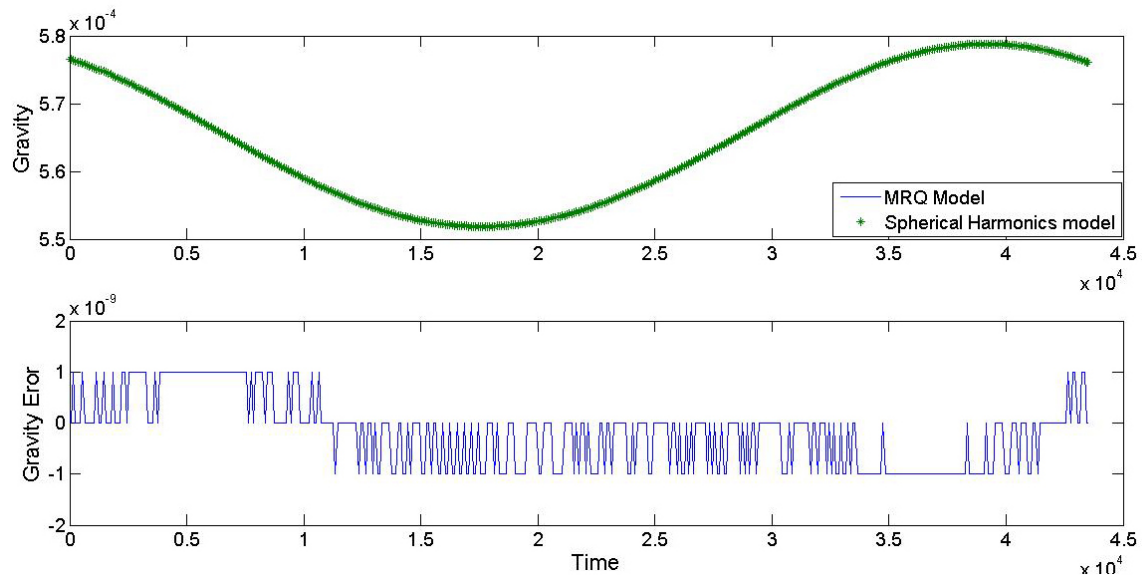


Figure 4.16. Plot showing the variation of gravity as predicted by the MRQ Sphere model and Spherical harmonics and the error between the two models.

With this plot we verify that the MRQ Sphere model is still consistent with the conventional model and proceed to the results. Thus verifying that the model becomes efficient with the increase in the radial distance.

4.3.2 Orbit Propagation

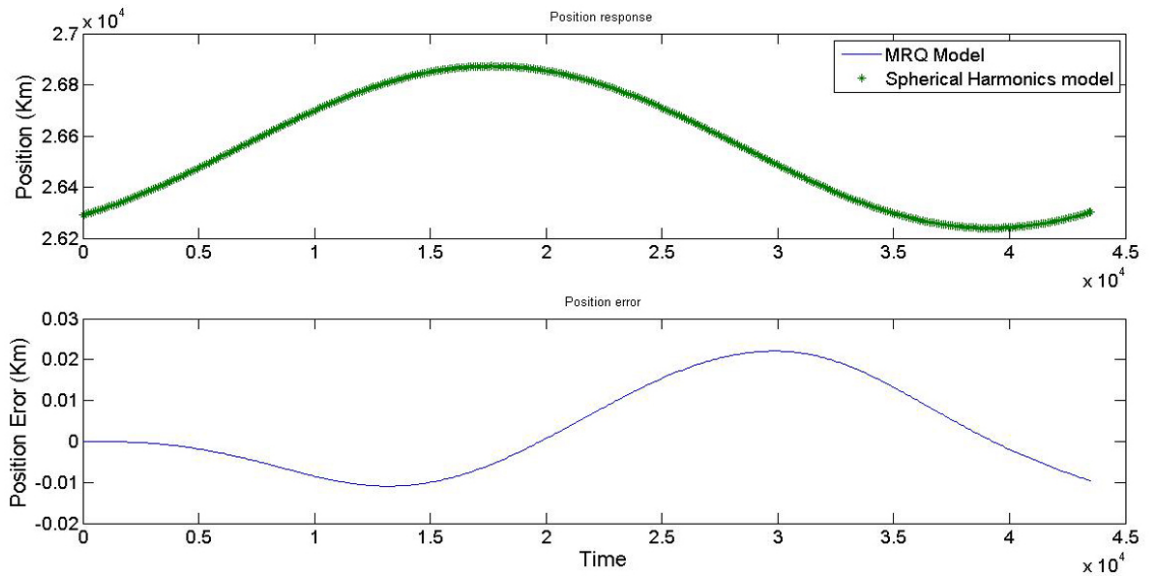


Figure 4.17. Plot showing the variation of position of GPS IIA-10 , as predicted by the MRQ Sphere model and Spherical harmonics and the error between the two models.

Fig. 4.17 shows the position of GPS BIIA-10 satellite with respect to time. We find that the error in the position predicted by the MRQ Sphere model and the spherical harmonics to be of the order of 0.02 Km as shown in the figure which can be accepted depending on the precision requirements of the application.

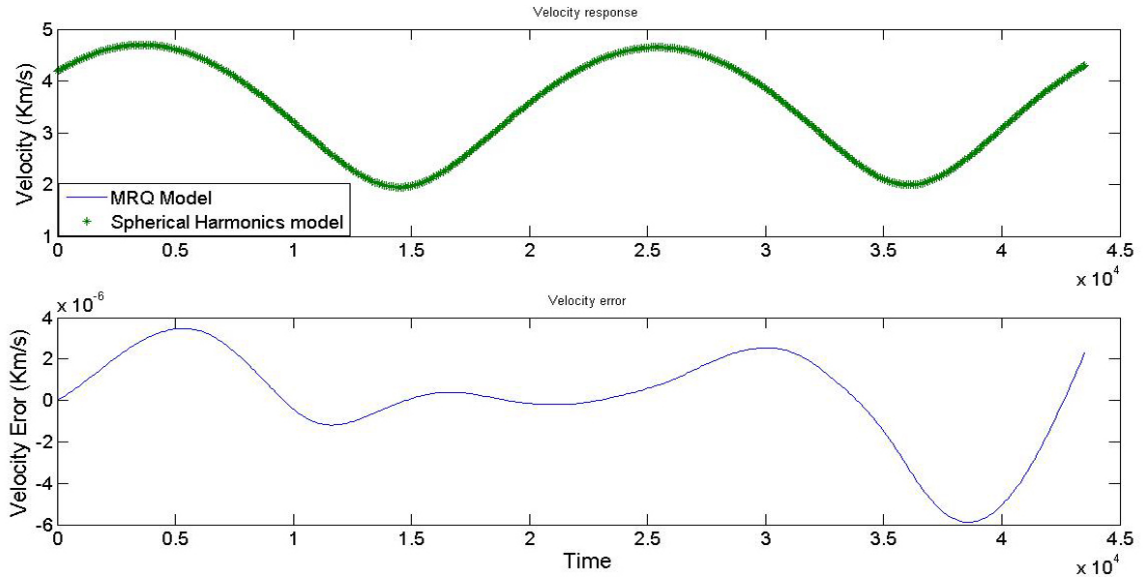


Figure 4.18. Plot showing the variation of velocity of GPS BIIA-10, as predicted by the MRQ Sphere model and Spherical harmonics and the error between the two models.

Fig. 4.18 shows the velocity response of GPS BIIA-10 satellite with respect to time. We find that the error in the velocity predicted by the MRQ Sphere model and the spherical harmonics to be of the order of 10^{-6} km/s as shown in the figure, which is considered acceptable to most of the applications.

4.3.3 Impact of the Number of Nodes

In order to investigate the impact of the number of nodes of the MRQ Sphere on the orbit propagation, we vary the number of nodes in the MRQ-sphere model. Instead of propagating the GPS BIIA-10 orbit with 372 nodes (16X16), we propagate it using 612 (20x20) nodes. We verify that after reaching the optimal number of nodes any increase will not effect the parameters as shown in Fig 4.19 and 4.20.

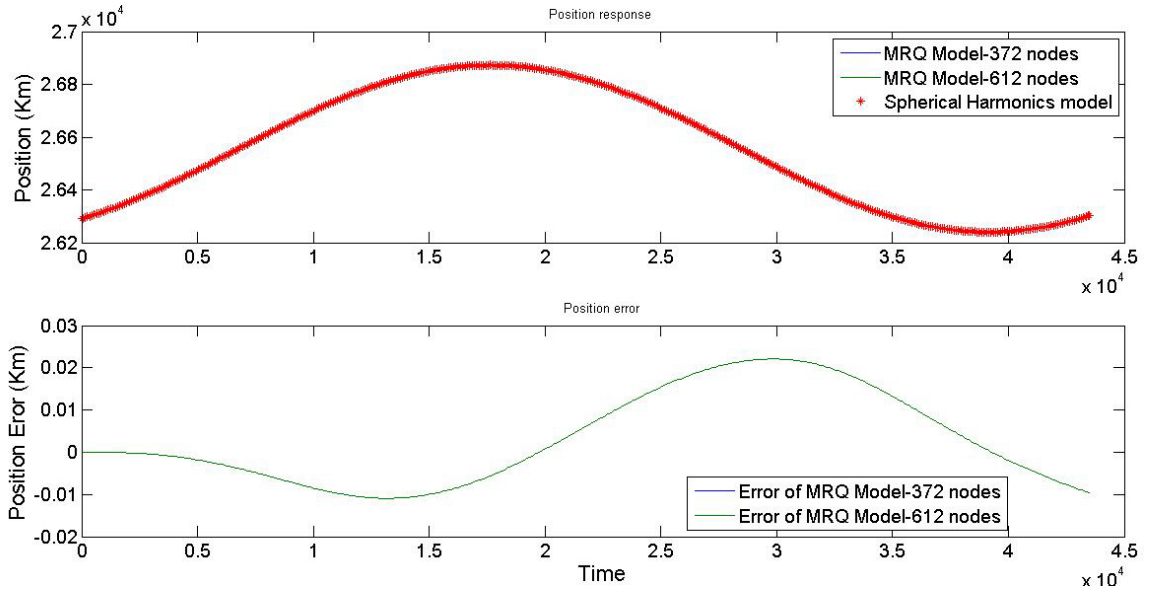


Figure 4.19. Plot showing impact of number of nodes on the position of the satellite predicted by the model.

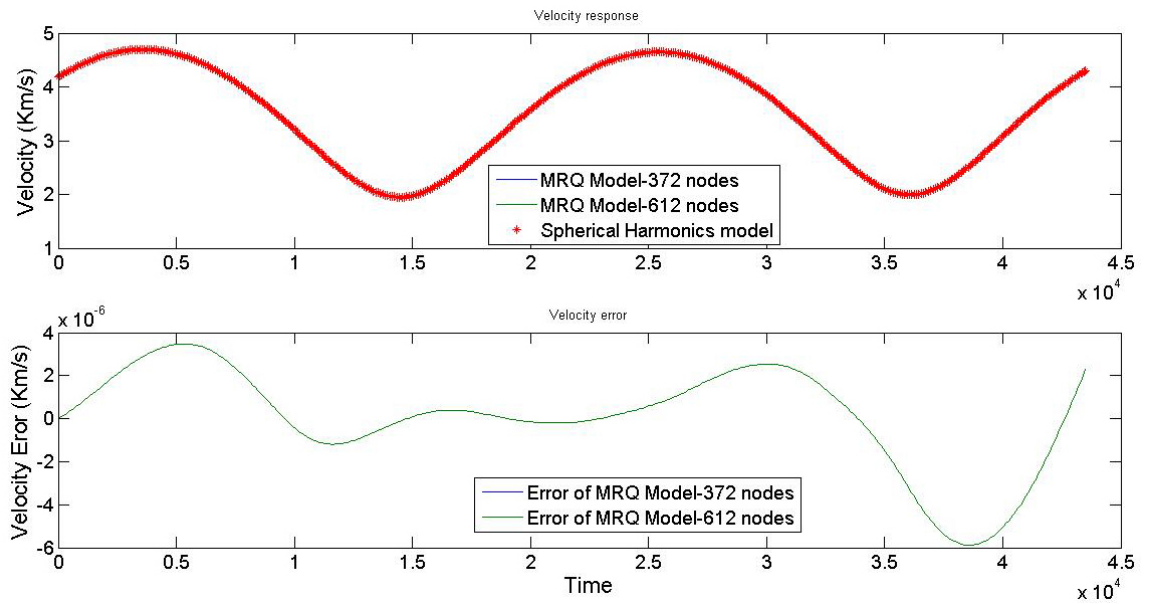


Figure 4.20. Plot showing impact of number of nodes on the velocity predicted by the model.

4.4 Computation Time

As mentioned earlier, the MRQ-Sphere method is not intended for fast evaluations of the gravity field[3]. In this section we provide a scope of comparison of the computation times of the orbit propagation using the MRQ-Sphere technique with that of the Spherical Harmonics. Table 4.1 shows the computation times that were recorded during the simulations.

Table 4.1. Propagation computation times recorded on an i-3 processor, with 4 gigabytes of RAM.

Satellite	MRQ Sphere	Spherical Harmonics
LAGEOS-II	473.8218 sec (25 shells)	56.6128 sec
LAGEOS-II	687.0284 sec (37 shells)	
GPS BIIA-10	325.4493 sec (372 nodes)	67.6576 sec
GPS BIIA-10	887.8265 sec (612 nodes)	

It can be verified here that the computation times scale along with the number of nodes and the number of shells. An increase in radial distance would increase the computation times in the spherical harmonic model due to increase in its orbital period; however, increasing the radial distance would decrease the computation times as seen in table 4.1. This is because increasing the radius results in fewer indicies to account for the radial decay, and it also reduces the number of nodes since the required degree of the model reduces with increasing radial distance.

4.5 Conclusion

The results show that the configuration of the current MRQ-sphere model which is efficient in the gravity estimation (Jones, 2010) [10], is also suitable for orbit propagation, depending on the precision of the model required as presented in chapter 3. However, an aspect of importance is the computation time. The time needed for the orbit propagation by MRQ-Sphere is high compared to the spherical harmonics model, and scales linearly with the nodes as they are used in the computation of the Z_j functions.

4.6 Future Work

Although quite efficient with its current configuration, the MRQ-sphere model should be adapted for usage in the field of Orbit propagation. The main goal would be to alter the representation for evaluation within the circumscribing sphere. Integrating the MRQ-Sphere model with the SRIF will further demonstrate the application of the model to the classic orbit estimation problem and provide a more realistic characterization of the model's estimation capabilities using radio science observations. A challenge in this task however, would be to define an algorithm to correct the estimation co-variance using the redistribution algorithm. Research to evaluate the MRQ-Sphere determined gravity field within the circumscribed sphere is ongoing.

REFERENCES

- [1] Arhens C.,Beylkin G. *Rotationally invariant quadratures for the sphere*. 2009.
- [2] Bate R.R., Mueller D.D., White J.E. *Fundamentals of Astrodynamics*. 1971.
- [3] Beylkin G.,Cramer R. *Towards Multiresolution estimation and efficient representation of gravitational fields*. 2002.
- [4] Beylkin G., Monzón L. *Approximation by exponential sums revisited*. 2010.
- [5] Fehlberg,E. *Classical Fifth-,Sixth-,Seventh-,Eighth-Order Runge Kutta formulas with step size control*. 1968.
- [6] Garmier R., Barriot J.P.,Kopnoliv A.S.,Yeomans D.K. *Modeling the EROS gravity field as an ellipsoidal harmonic expansion from the near Earth doppler tracking data*. 2002.
- [7] Gottlieb R.G. *Fast Gravity, Gravity Partial, Normalized Gravity, Gravity sient Torque and Magnetic Field: Derivation, Code and Data*. 1993.
- [8] Gradshteyn I.S., Ryzhik I.M., *Table of Integrals, Series and Products,7th Edition*. 2007.
- [9] Jekeli C. *Potential Theory and Static Gravity Field of the Earth*. 2007.
- [10] Jones B.A., Beylkin G., Born G.H., Provence R.S. *A Multiresolution model for small body gravity estimation*. 2010.
- [11] Kopnoliv A.S.,Asmer S.W.,Carranza E., Sjogren W.,Yuan D. *Recent gravity Models as a result of the Lunar Prospector Mission*. 2001.
- [12] Kopnoliv A.S.,Miller J.K., Owen W.M., Yeomans D.K., Giorgini J.D. *A global solution for the gravity field,rotation,landmarks and emphemeris of Eros*. 2002.

- [13] Petit G., Luzum B. *IERS Conventions*. 2010.
- [14] Sezgö *Orthogonal Polynomials*. 1975.
- [15] Tapley B.D., Schutz B.E., Born G.H *Statistical Orbit Determination, 1st Edition*. 2004.
- [16] Thompson W.T *Introduction to Space Dynamics*. 1986.
- [17] Tsoulis D., Jamet O., Verdun J., Gonindard N. *Recursive algorithms for the computation of the potential harmonic coefficients of a constant density polyhedron*. 2009.

